NASA/TM-2004-213235
ARL-TR-3130

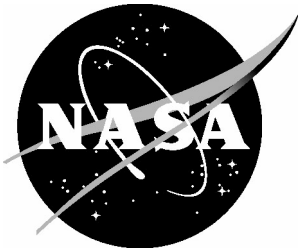

Nondestructive Evaluation (NDE) Results on Sikorsky Aircraft Survivable Affordable Reparable Airframe Program (SARAP) Samples

Joseph N. Zalameda and Robert F. Anastasi
U.S. Army Research Laboratory
Vehicle Technology Directorate
Langley Research Center, Hampton, Virginia

Eric I. Madaras
Langley Research Center, Hampton, Virginia

August 2004

The NASA STI Program Office . . . in Profile

Since its founding, NASA has been dedicated to the advancement of aeronautics and space science. The NASA Scientific and Technical Information (STI) Program Office plays a key part in helping NASA maintain this important role.

The NASA STI Program Office is operated by Langley Research Center, the lead center for NASA's scientific and technical information. The NASA STI Program Office provides access to the NASA STI Database, the largest collection of aeronautical and space science STI in the world. The Program Office is also NASA's institutional mechanism for disseminating the results of its research and development activities. These results are published by NASA in the NASA STI Report Series, which includes the following report types:

- TECHNICAL PUBLICATION. Reports of completed research or a major significant phase of research that present the results of NASA programs and include extensive data or theoretical analysis. Includes compilations of significant scientific and technical data and information deemed to be of continuing reference value. NASA counterpart of peer-reviewed formal professional papers, but having less stringent limitations on manuscript length and extent of graphic presentations.

- TECHNICAL MEMORANDUM. Scientific and technical findings that are preliminary or of specialized interest, e.g., quick release reports, working papers, and bibliographies that contain minimal annotation. Does not contain extensive analysis.

- CONTRACTOR REPORT. Scientific and technical findings by NASA-sponsored contractors and grantees.

- CONFERENCE PUBLICATION. Collected papers from scientific and technical conferences, symposia, seminars, or other meetings sponsored or co-sponsored by NASA.

- SPECIAL PUBLICATION. Scientific, technical, or historical information from NASA programs, projects, and missions, often concerned with subjects having substantial public interest.

- TECHNICAL TRANSLATION. English-language translations of foreign scientific and technical material pertinent to NASA's mission.

Specialized services that complement the STI Program Office's diverse offerings include creating custom thesauri, building customized databases, organizing and publishing research results ... even providing videos.

For more information about the NASA STI Program Office, see the following:

- Access the NASA STI Program Home Page at ***http://www.sti.nasa.gov***

- E-mail your question via the Internet to help@sti.nasa.gov

- Fax your question to the NASA STI Help Desk at (301) 621-0134

- Phone the NASA STI Help Desk at (301) 621-0390

- Write to:
  NASA STI Help Desk
  NASA Center for AeroSpace Information
  7121 Standard Drive
  Hanover, MD 21076-1320

NASA/TM-2004-213235
ARL-TR-3130

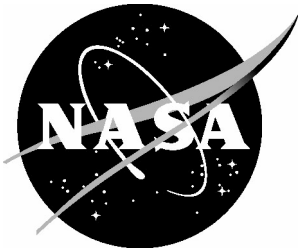

Nondestructive Evaluation (NDE) Results on Sikorsky Aircraft Survivable Affordable Reparable Airframe Program (SARAP) Samples

Joseph N. Zalameda and Robert F. Anastasi
U.S. Army Research Laboratory
Vehicle Technology Directorate
Langley Research Center, Hampton, Virginia

Eric I. Madaras
Langley Research Center, Hampton, Virginia

National Aeronautics and
Space Administration

Langley Research Center
Hampton, Virginia 23681-2199

August 2004

Available from:

NASA Center for AeroSpace Information (CASI)
7121 Standard Drive
Hanover, MD 21076-1320
(301) 621-0390

National Technical Information Service (NTIS)
5285 Port Royal Road
Springfield, VA 22161-2171
(703) 605-6000

SUMMARY

The Survivable, Affordable, Reparable Airframe Program (SARAP) will develop/produce new structural design concepts with lower structural weight, reduced manufacturing complexity and development time, increased readiness, and improved threat protection. These new structural concepts will require advanced field capable inspection technologies to help meet the SARAP structural objectives. In the area of repair, damage assessment using nondestructive inspection (NDI) is critical to identify repair location and size. Also NDI is necessary to assess the quality of the finished repair and repair integrity during use. The NDI technologies must be portable and field capable, rapid, quantitative, user friendly, and able to inspect complex geometries. The purpose of this work is to conduct an assessment of new and emerging NDI methods that can potentially satisfy the SARAP program goals. This research was supported and by Sikorsky Aircraft and the Aviation Applied Technology Directorate under Technology Investment Agreement No. DAAH10-02-2-0001. For this evaluation three composite material test panels were obtained from Sikorsky Aircraft. The first panel was a flat honeycomb core sandwich panel with painted and unpainted sides to concurrently evaluate any inspection limitations due to low infrared (IR) MIL-C-46168 exterior aircraft paint, the second panel was an X-Cor™ advanced sandwich panel and the third panel was a double ramped honeycomb sandwich panel with a co-cured T-blade stiffener. The NDI technologies evaluated were thermography, laser ultrasound, and Lamb wave ultrasound.

Single side and through transmission thermal inspections using flash and quartz heat lamps were performed on all three of the samples provided by Sikorsky. For the honeycomb sandwich panel, all the foreign object inserts and impact damage defects were detected although the smallest impact energy defects were barely detectable. In addition, the low reflectivity paint coating on half of the panel, did not adversely effect the thermal inspection but in some cases enhanced it. A quartz lamp was necessary to heat through the honeycomb. The heat was able to propagate through the honeycomb and a through transmission diffusivity image was generated on the honeycomb panel. This is significant because the potential to detect damage on the opposite side from the heat source may be possible for honeycomb structures. All the impact damage and pull pin defects were detected on the X-Cor™ advanced sandwich panel although the smallest pull pin defects were more easily detected on the back side. Through transmission quartz lamp results easily detected all the pull pin defects, however the impact damage was barely detectable. The smallest T-blade side impact was not detected which could possibly indicate no damage. Close up single side thermal inspections were performed on the two impacted areas on the middle T-blade of the double ramped sandwich panel and successfully showed damaged areas. Through transmission thermal diffusivity images using the flash lamp were generated on the middle defects on the T-blade and compared well with previous damage measurements. The impact damage defects were clearly seen along with the largest foreign object inserts. The smallest foreign object inserts were not clearly seen due to the blade thickness. Overall thermography was able to rapidly detect most of the defects.

Laser based ultrasonic C-scans were most promising on the T-blade area on the double ramped panel. The images show the loss of echo in the T-blade web area, the 10 ft-lb impact, and two embedded defects. Scans around the 5 ft-lb impact show the loss of echo in the T-blade web

area, two embedded defects, and the 5 ft-lb impact. These images showed that the general structure in the T-blade could be seen in the generated C-scan images and that it was possible to observe 0.025 centimeters thickness changes in this structure. Inserts near the T-blade flange back surface were readily seen, but inserts near the flange front surface were obscured in part from the laser ultrasound generation. The impact damage area for the 10 ft-lb site was readily seen, but the front surface damage was partially hidden by the laser ultrasound generation signal. In general the laser-based ultrasound appears to be a viable method for inspecting the T-blade for thickness variations and more extensive impact damage.

All three of the samples provided by Sikorsky were tested with an ultrasonic Lamb wave system. The panels were scanned in sections approximately 30 by 30 centimeters with 2.54 centimeters incremental steps. Ultrasonic Lamb wave results on the T-stiffened area showed material thickness changes in addition to the possible defect locations. It is noted that the frequency selection and scanning resolution chosen limited the defect resolution. By optimizing these parameters improved defect contrast could possibly be obtained.

Based on the results obtained in this study, thermography proved best overall because of its ability to detect the defects of interest as compared to the other technologies. In addition to thermography's field portability potential, the inspection technology is safe, one sided, noncontact and provides rapid full field imaging. Laser ultrasound has possibilities in limited applications, however field portability issues may restrict the technology to depot applications. Recent advances in miniature laser diode technology may result in future field portable systems. The ultrasonic Lamb wave technique gave the weakest results particularly on the thin skin panels. Ultrasonic Lamb wave measurements on the thicker double ramped T-stiffened area showed possible defect locations, however the lack of defect contrast on the other samples was disappointing. It is noted that the frequency selection and scanning resolution may have contributed to this. Lamb wave measurements were particularly difficult on samples with thin skins because of the low frequencies used. Since existing equipment was used, transducers more suited for thicker structures were only available. By optimizing the frequency and transducer size, improved defect contrast could possibly be obtained.

INTRODUCTION

The Survivable, Affordable, Reparable Airframe Program (SARAP) will develop/produce new structural design concepts with lower structural weight, reduced manufacturing complexity and development time, increased readiness, and improved threat protection. These new structural concepts will require advanced field capable inspection technologies to help meet the SARAP structural objectives. In the area of repair, damage assessment using nondestructive inspection (NDI) is critical to identify repair location and size. Also NDI is necessary to assess the quality of the finished repair and repair integrity during use. The NDI technologies being considered must be portable and field capable, rapid, quantitative, user friendly, and able to inspect complex geometries. The NDI technologies must be practical, economical, and be robust in the Army field environment. The purpose of this work is to conduct an assessment of new and emerging NDI methods that can potentially satisfy the SARAP program goals. The NDI technologies evaluated were thermography, laser ultrasound, and Lamb wave ultrasound.

The advantages of thermography are noncontact, rapid inspection, single side, and imaging of large areas. The technique is safe where only a small amount of heat (typically less than 15 degrees Celsius above ambient) is applied to the surface of the structure. The temporal temperature response can be fitted to a theoretical model for a quantitative measurement of thermal diffusivity or thickness. Thermal diffusivity is an important material property for quantitative thermal nondestructive evaluation. Any change in this material property can potentially be attributed to a defect [1]. Some types of defects that can affect thermal diffusivity are delaminations, fiber volume fraction, disbonds, matrix and fiber cracking, and gross porosity. Two types of heat sources commonly used to measure thermal diffusivity are flash and quartz lamps. Flash lamps produce a very short duration intense pulse of heat flux (impulse heating), while quartz lamps are lower cost and also a common excitation source for thermal inspection systems. In comparison to flash lamps, which produce a short duration heat flux, quartz lamps produce a long pulse of heat flux (step heating) which allows for the delivery of larger amounts of energy. Quartz lamps are more useful for the inspection of thicker structures or through the thickness of honeycomb core sandwich structures. Thermography measurements were performed on three samples received from Sikorsky Aircraft. Through transmission thermal measurements were performed using both flash and quartz lamp heating techniques and also single sided thermal measurements were performed using flash heating.

Laser based ultrasound is a non-contact inspection technology that uses a laser to generate ultrasound and a laser-interferometer system to measure ultrasonic surface vibrations [2,3]. The ultrasound is generated using a high-power pulsed laser and is usually detected by a Fabry-Perot interferometer. The ultrasonic generation mechanism involves rapidly heating a small area with laser light. When the laser energy is below material damage threshold the mechanism is referred to as being in the thermoelastic regime and when over this threshold the ablation regime. For non-destructive inspection the thermoelastic regime is preferred. For ultrasonic detection a continuous wave laser is typically used in conjunction with an interferometer. Light from the detection laser is scattered or reflected by the material surface and part of that light is detected and transformed by the interferometer into an ultrasonic A-scan signal that can be processed in the time and frequency domain. To generate an ultrasonic C-scan

or B-scan images a series of point measurements are taken by typically scanning the laser beams over the material surface. This laser generation and detection of ultrasound is performed without mechanical contact to the inspection material as opposed to conventional ultrasonic techniques that require some form of mechanical contact. This non-contact nature of the technique is the prime advantage that laser-based ultrasound has over conventional ultrasound.

Ultrasonic Lamb or plate waves have an advantage over conventional through-the-thickness ultrasound because the energy can be transmitted over greater distances. This involves the use of two transducers: one operating as a pitch and the other as a catch transducer. For a known distance the velocity can be measured and this velocity is dependent on the properties of the material or structure [4]. The Lamb wave velocity is sensitive to the in-plane elastic properties of the material. This technology has been used to investigate porosity, fiber volume fraction, and matrix cracking.

SAMPLES

Three samples were obtained from Sikorsky Aircraft. The first panel was a flat sandwich panel with honeycomb core, the second panel was an X-Cor^{TM} advanced sandwich panel and the third panel was a double ramped honeycomb sandwich panel with a cocured T-blade stiffener. The honeycomb core sample was 61 centimeters by 61 centimeters in size with 2 ply skins sandwiching the honeycomb. The defect layout is shown in figure 1. For a comparison the left side of the panel was unpainted and the right side of the panel was coated with a low infrared MIL-C-46168 exterior aircraft paint. The sample contained impact damage and Fluorinated Ethylene Propylene (FEP) insert defects (0.0025 cm thick) buried underneath the skin. The second panel inspected was the X-Cor^{TM} advanced sandwich panel. This panel was 30.5 centimeters by 30.5 centimeters in size with four impact damage sites (6.0, 4.5, 3.5, and 2.5 ft-lb impact energies) and pull pin defects. The defect layout is shown in figure 2. The last sample inspected was the double ramped sandwich panel with a cocured T-blade stiffener. This sample was 50.8 centimeters by 96.5 centimeters in size and contained FEP insert defects (0.0025 cm thick) and impact damage defects (10.0 and 5.0 ft-lb impact energies). The defect layout of the top and side views are shown in figures 3 and 4 respectively.

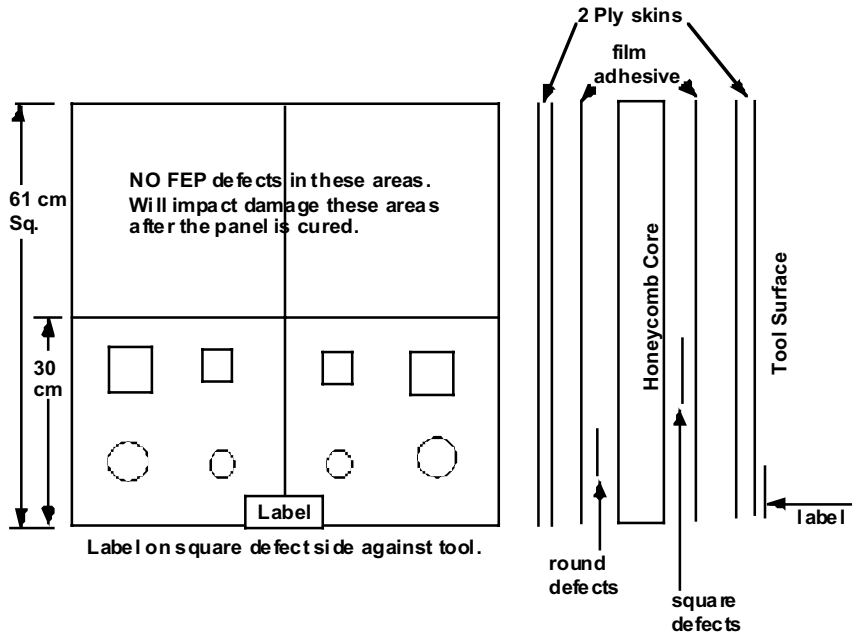

Figure 1: Defect layout of honeycomb core sample.

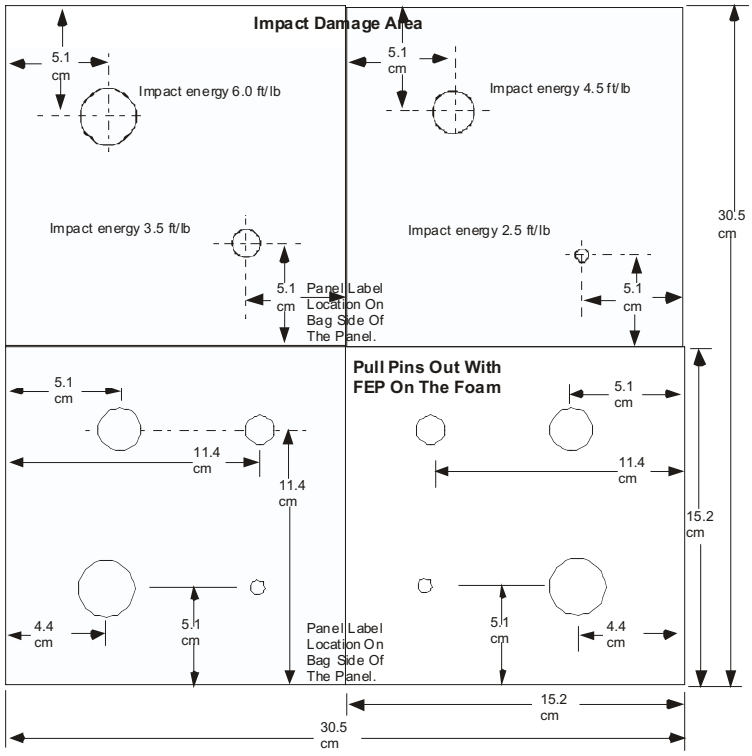

Figure 2: Defect layout of X-Cor™ advanced sandwich panel.

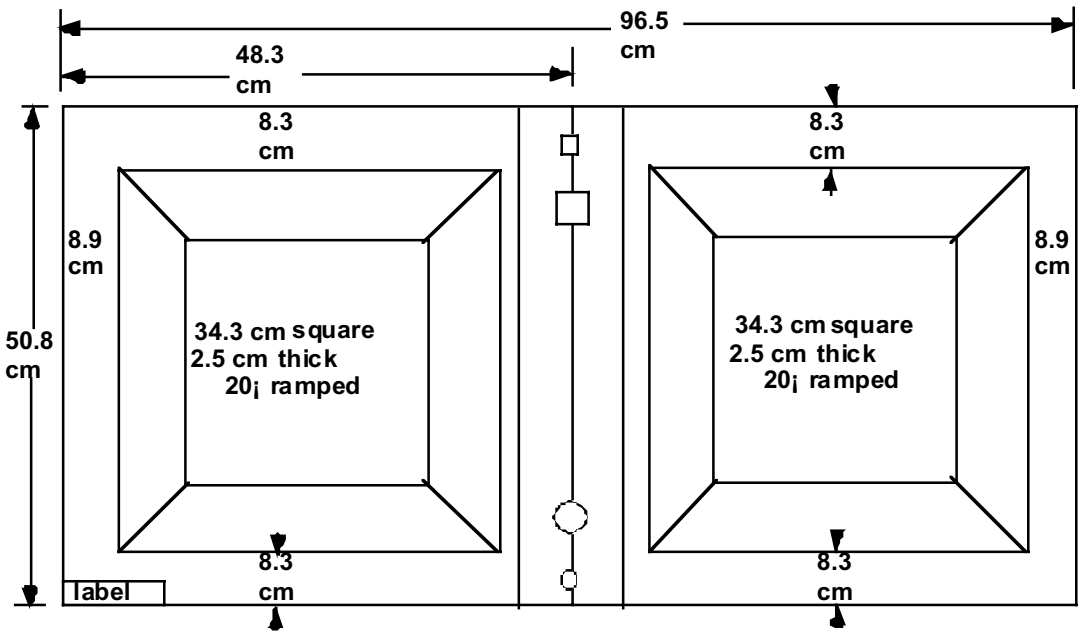

Figure 3: Defect layout of double ramped sandwich panel with cocured T-stiffener blade.

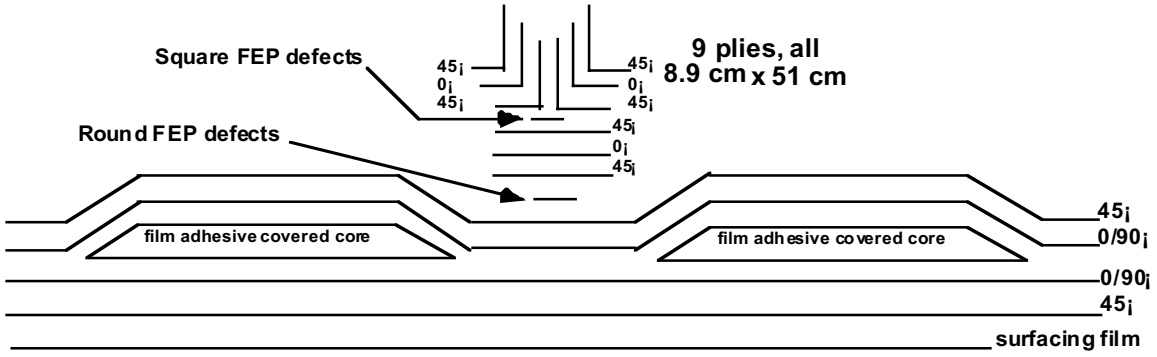

Figure 4: Side view of defect layout of double ramped sandwich panel with cocured T-stiffener blade.

THERMOGRAPHY

The infrared camera used for through transmission measurements was a 256 x 256 cooled focal plane array operating in the 3 – 5 micrometer wavelength band. The infrared camera used for the single sided measurements was a cooled 256 x 320 focal plane array operating in the 3 – 5 micrometer wavelength band. The acquired data sets were composed of a series of 16 bit digital images captured at 1/60 of a second. A computer (desktop or laptop) was used to trigger the heat lamps and acquire the data through a data acquisition card made by Bitflow. Thermal Imaging Analysis (TIA) software developed by NASA was used to control the inspection parameters, storage of data, and subsequent data analysis. Two types of heat sources were used: flash lamps and quartz lamps. The flash lamps were commercially available photographic systems with a 6400 Watt seconds power supply. The total system cost is approximately $65K (55K for infrared camera). The quartz lamps were also commercially available linear tubes rated at 500 watts. The single side thermography setup is shown in figure 5. A theoretical 1-dimensional analytic solution is fitted to the thermal data to obtain values of effective thermal diffusivity [5]. The single side analytic solution used is a function of the thickness and thermal diffusivity. The single side heating temperature response equation assumes no convection losses and the flash duration is considered instantaneous for the samples inspected. An example of the model fit to the data is shown in figure 6 and the agreement is very good. The temperature response equation assumes no convection losses and the flash duration is considered instantaneous for the samples inspected. The through transmission setup is shown in figure 7. A theoretical 1-dimensional single layer analytic solution is fitted to the thermal data to obtain values of effective thermal diffusivity for the through transmission measurement [5]. The analytic solution used is also a function of both the thickness and thermal diffusivity. For quartz lamp inspections analytic solution is integrated over the heating period and then fitted to the data. The time required to do this fitting analysis is on the order of around 5 - 10 minutes using a compiled C routine.

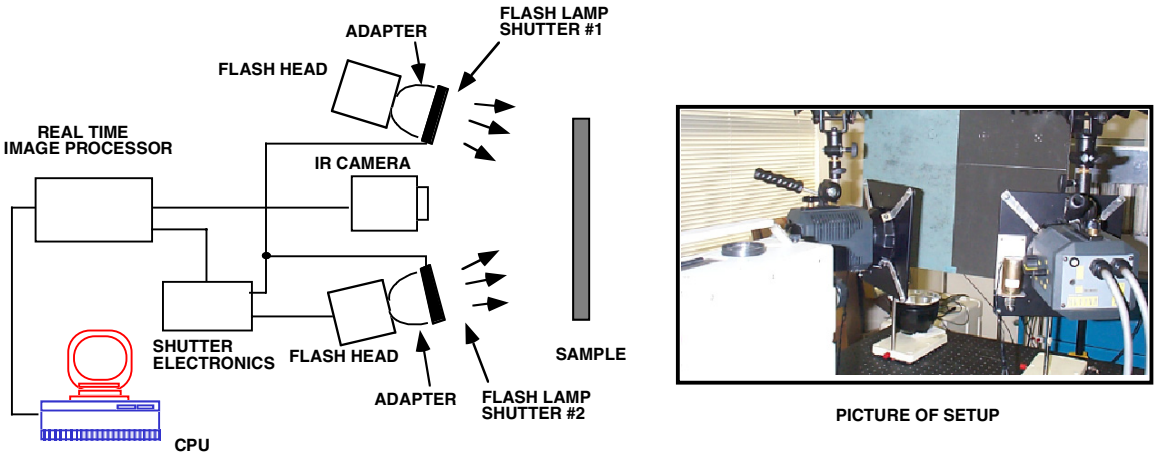

Figure 5: Single side thermography setup.

Another algorithm used is image normalization. Image normalization is an image processing technique where the sum (average) of the total images to be processed is divided by the averaged set of images where the defect is observed in the temperature data [6]. This simple calculation minimizes uneven heating and emissivity variations while improving defect contrast. This processing technique doesn't provide a quantitative material property measurement like the model fitting diffusivity calculation previously discussed, however the computation times are on the order of less than 20 seconds.

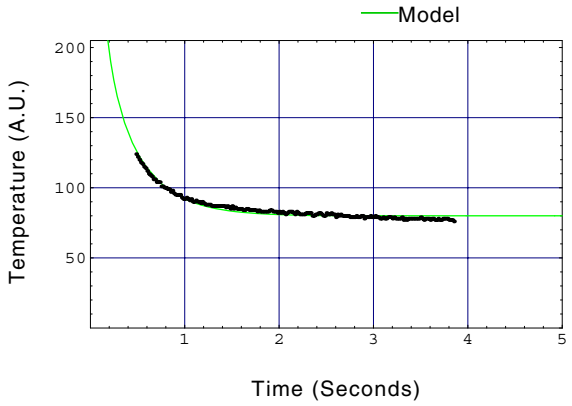

Figure 6: Example of model fit to the data.

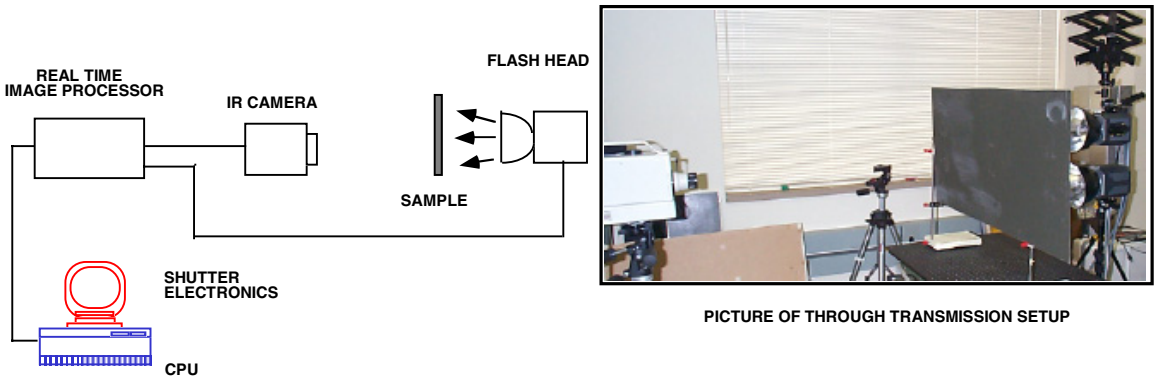

Figure 7: Through transmission thermography setup.

Single Side Thermal Inspections

The thermal measurements of the honeycomb panel was broken up into 6 inspection areas and the setup shown in figure 5 was used. The inspection views are marked in figure 8. The inspection parameters were 240 frames acquired at 60 frames per second digital infrared camera

output for a total inspection time per view of 4 seconds. The inspection images for areas I, II, III, IV, V, and VI are shown in figures 9, 10, 11, 12, 13, and 14 respectively and clearly show the underlying core. Quantitative effective diffusivity algorithm was used to generate the images in figures 9 and 10 and an image normalization alogorithm was used to generate images in figures 11, 12, 13, and 14. The inspection images for areas I and II clearly showed impact damage for all but the lowest impacts (2.5 ft-lbs). The impact damage can be seen by lower diffusivity values (darker areas) due to the lower thermal conductivity caused by fiber/matrix cracking and core crushing. Closer inspection of the impact damage areas shows core seperation from the skin (figure 10). The painted side provided better defect signal to noise with the lowest impact barely visible. The FEP inserts were all detected in figures 11 – 14.

Shown in figures 15 and 16 are the thermal diffusivity images of the front and back side of the X-Cor™ advanced sandwich panel with impact damage and pull pin defects. The inspection parameters were 300 frames acquired at 60 frames per second digital infrared camera output for a total inspection time per view of 5 seconds. The impact damage areas, shown by the lower diffusivity values, were all detected in figure 15. The pull pin defects show up as light areas due to the lower thermal mass (material thickness) due to material removal. The back side inspection (figure 16) shows the smallest pull pin defect.

The single side thermal measurements of the double ramped sandwich panel with T-Blade were broken up into 3 inspection areas. The inspection views are marked in figure 17. The inspection parameters were 600 frames acquired at 60 frames per second digital infrared camera output for a total inspection time per view of 10 seconds. The quantitative effective diffusivity inspection images for areas I, II, and III are shown in figures 18, 19, and 20 respectively. Also shown in figure 20 are closeup single side diffusivity images of the middle impacts in area III. Again the impact damage areas are shown by the lower diffusivity values.

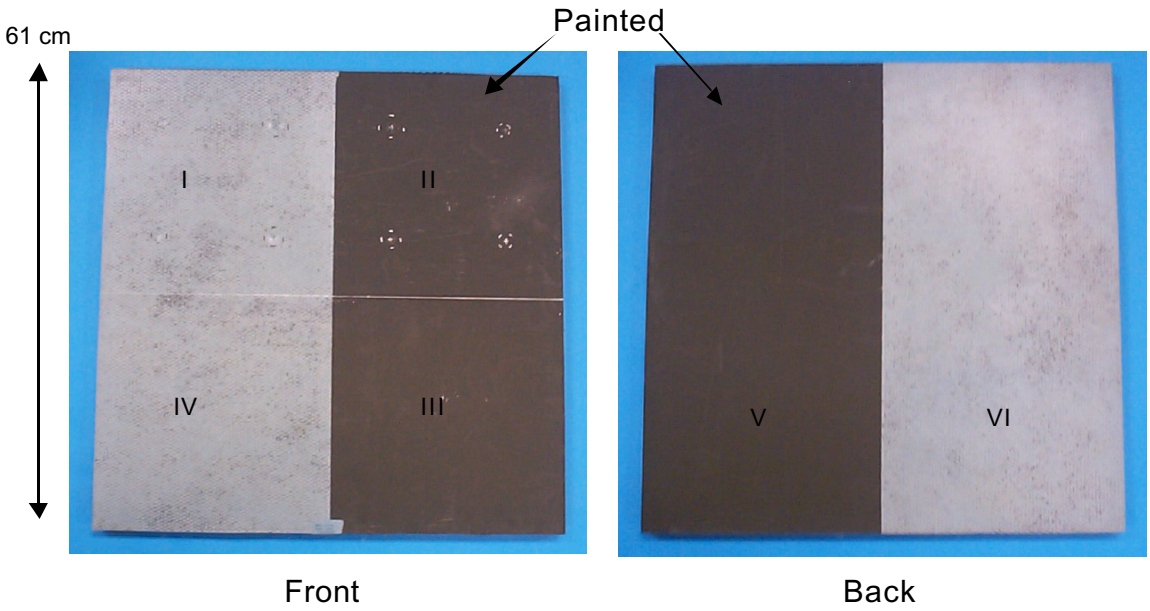

Figure 8: Front and back views of honeycomb sample with designated inspection areas.

No damage was detected for the two lower impact energy areas as shown in figure 18 and this may be due to no actual damage. The left side impacts in figure 19 showed areas of lower diffusivity due to the impact damage. A close up of the middle impacted areas (figure 20) barely show delamination damage protruding to the right side of the impact site for both impact energies.

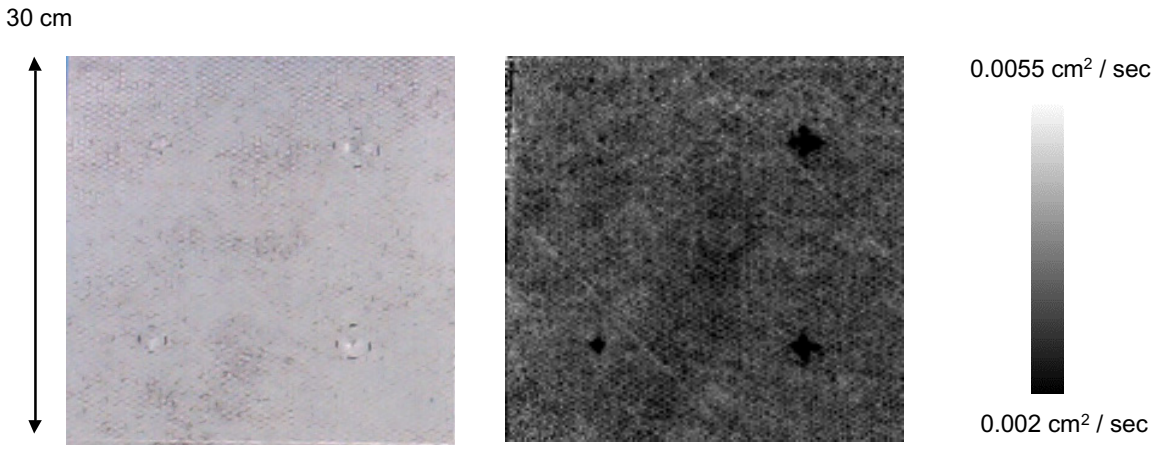

Figure 9: Visual and thermal diffusivity inspection image of area I of the honeycomb sample.

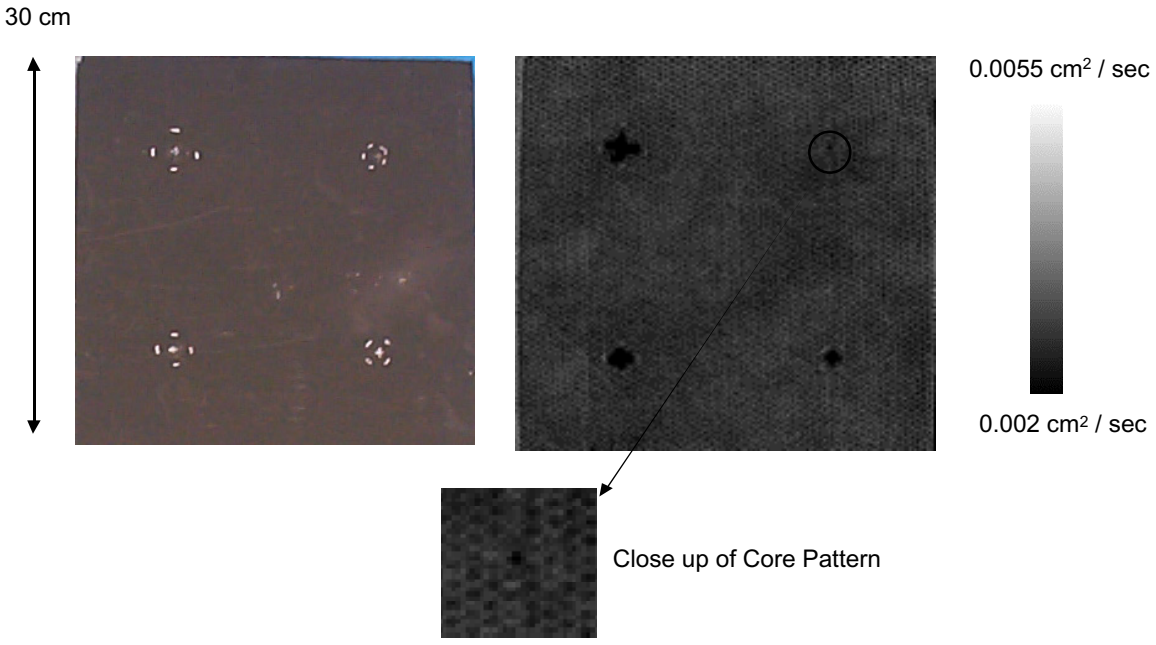

Figure 10: Visual and thermal diffusivity inspection image of area II of the honeycomb sample.

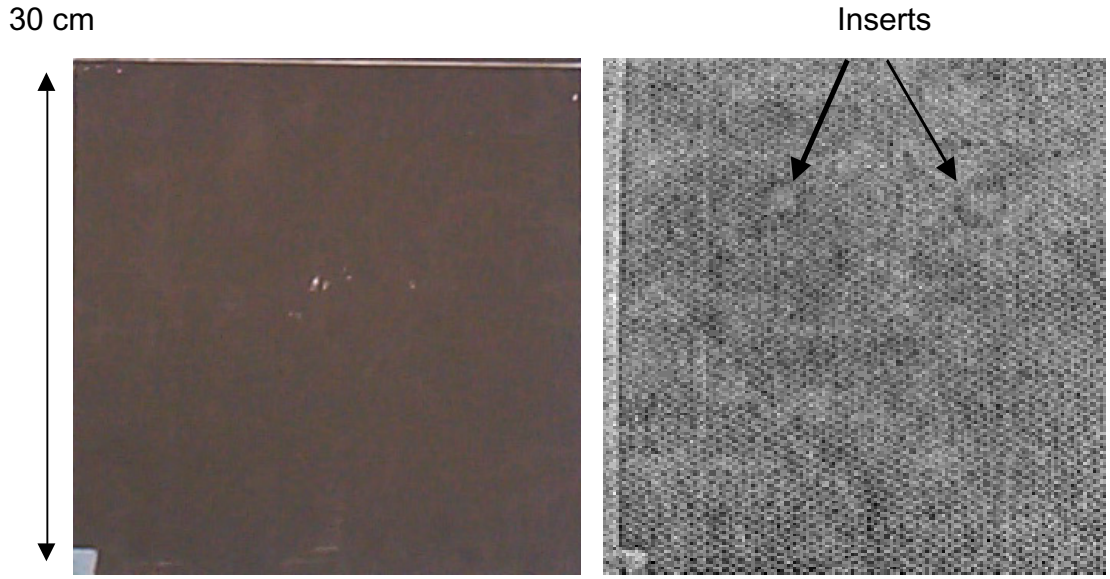

Figure 11: Visual and thermal normalization inspection image of area III of the honeycomb sample.

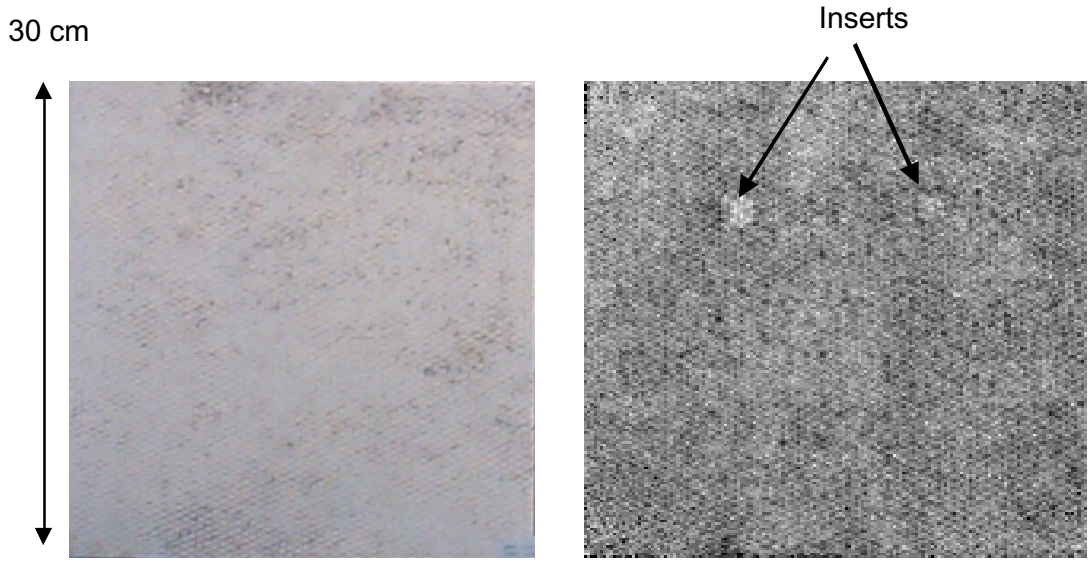

Figure 12: Visual and thermal normalization inspection image of area IV of the honeycomb sample.

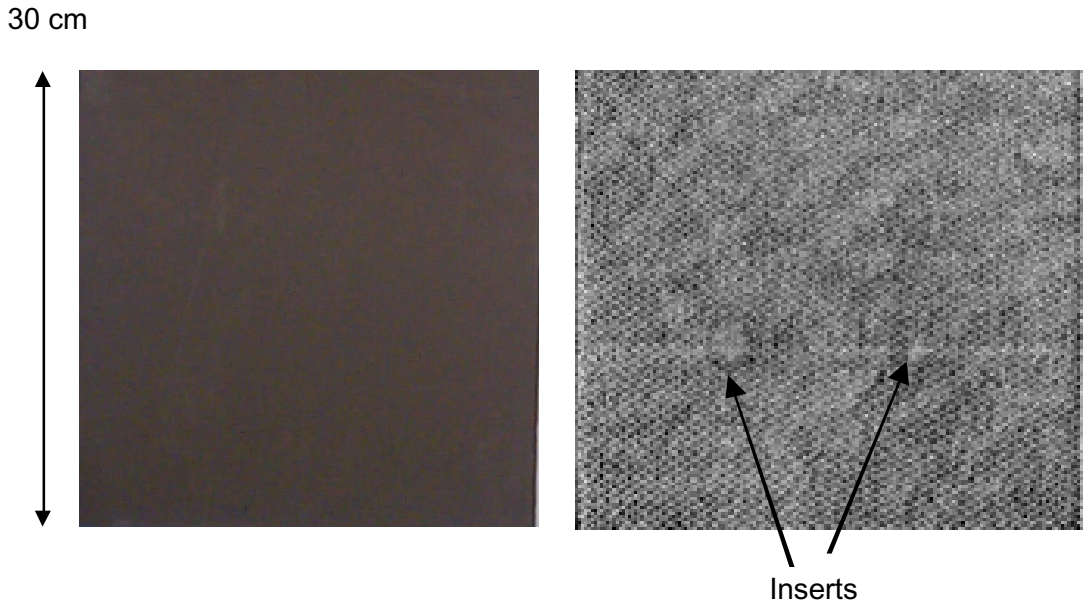

Figure 13: Visual and thermal normalization inspection image of area V of the honeycomb sample.

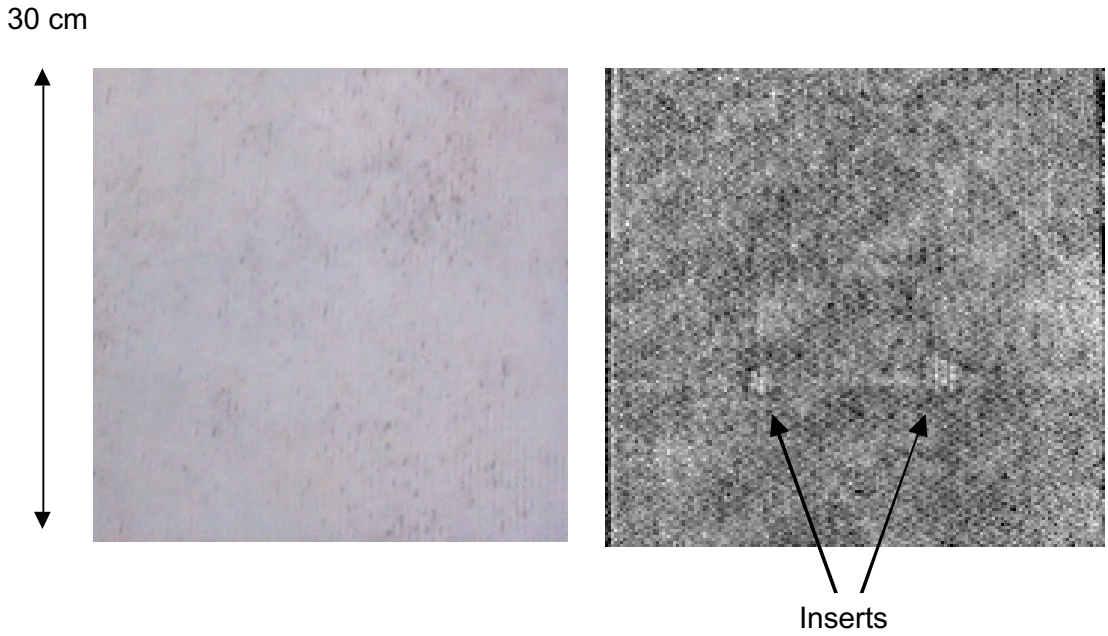

Figure 14: Visual and thermal normalization inspection image of area VI of the honeycomb sample.

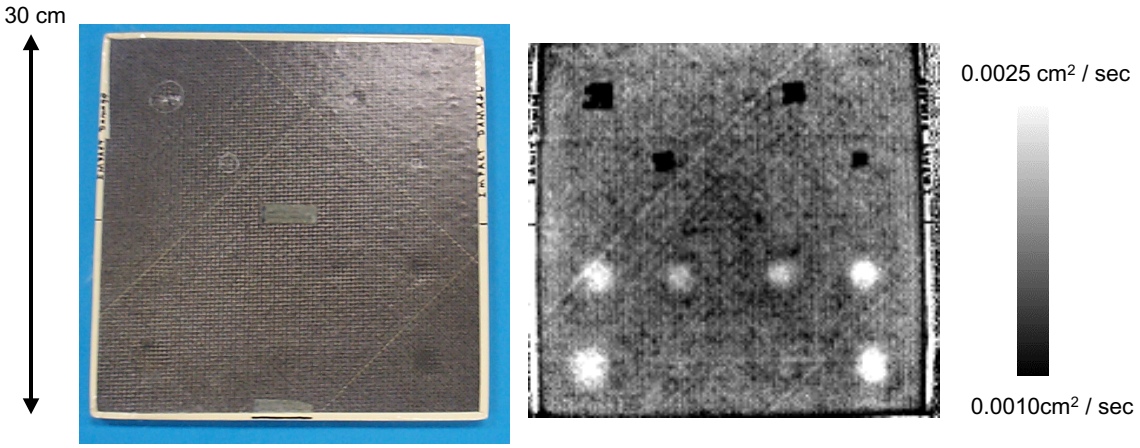

Figure 15: Visual and thermal diffusivity inspection image of front side of X-Cor™ advanced sandwich panel.

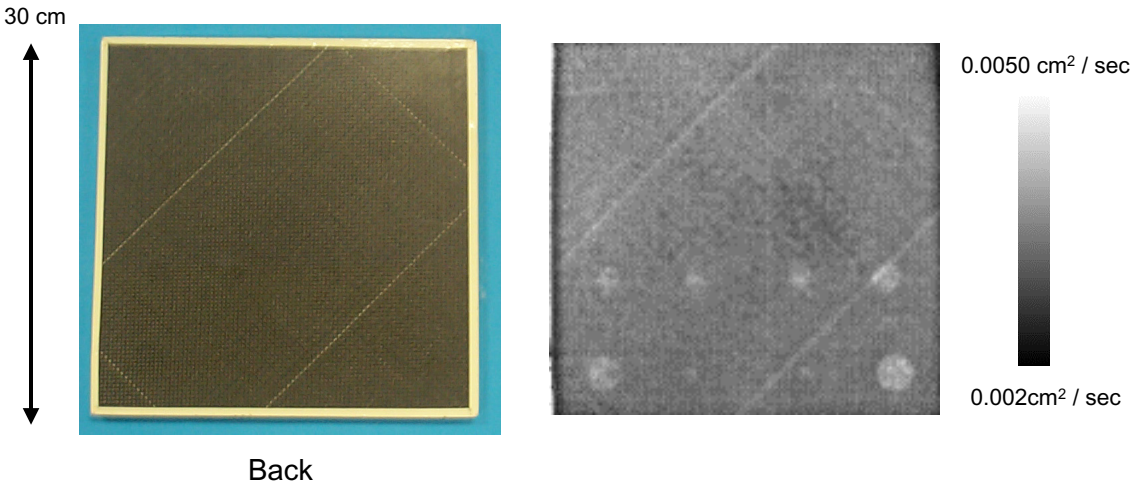

Figure 16: Visual and thermal diffusivity inspection image of back side of X-Cor™ advanced sandwich panel.

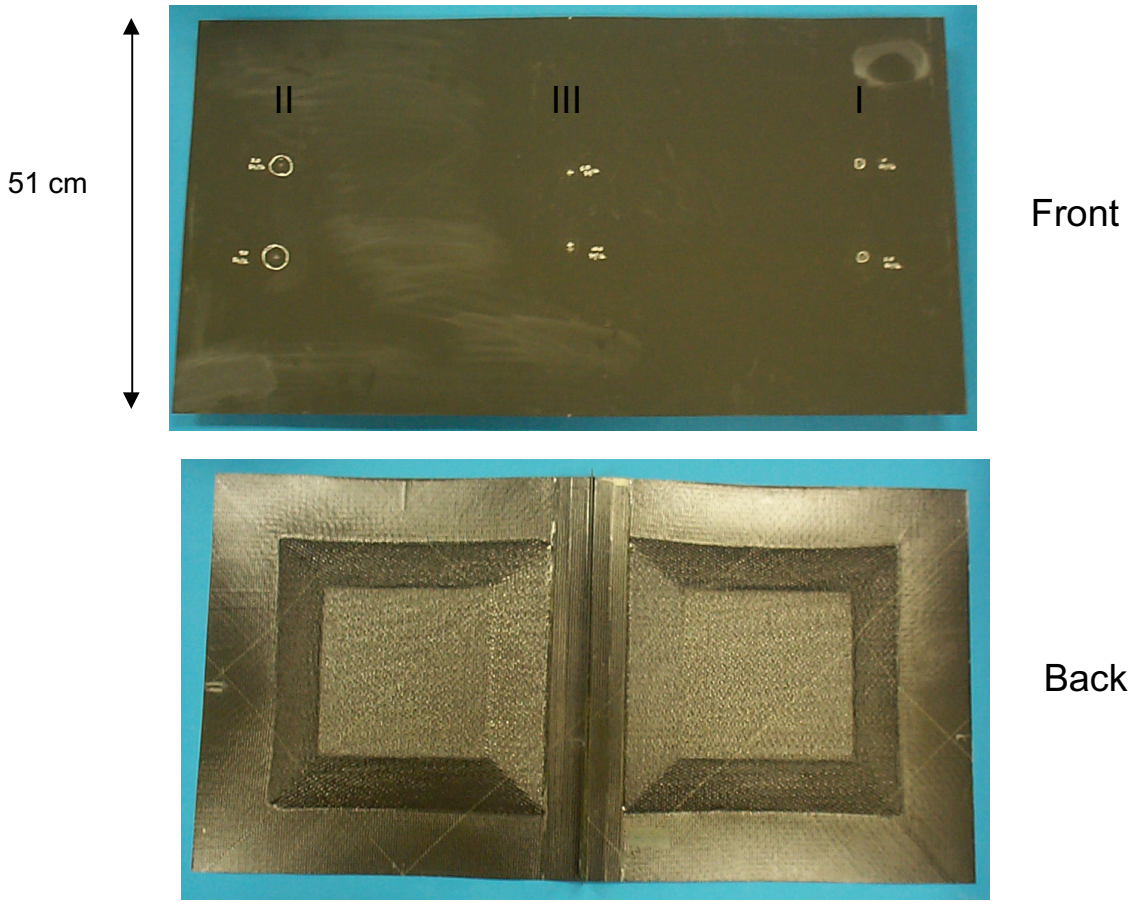

Figure 17: Picture of double ramped sandwich panel with T-Blade.

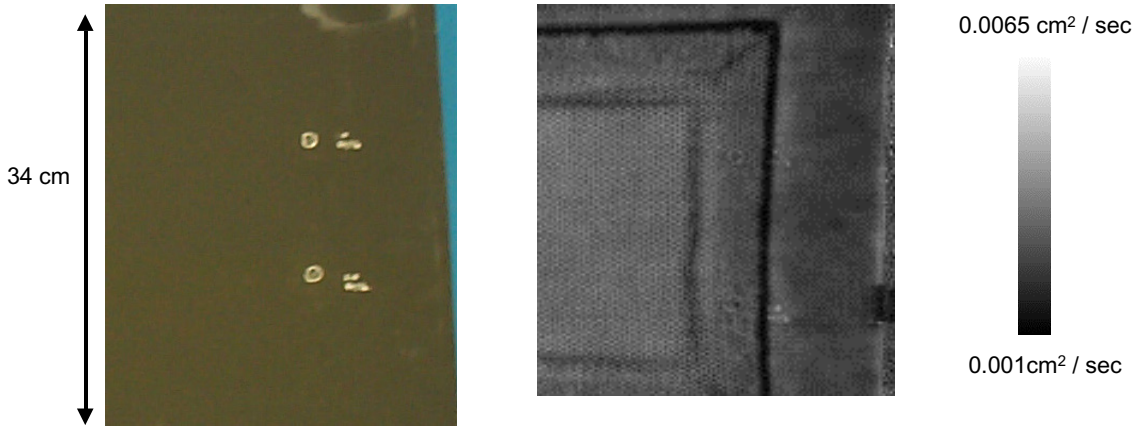

Figure 18: Visual and thermal diffusivity inspection image of right side impacts (area I).

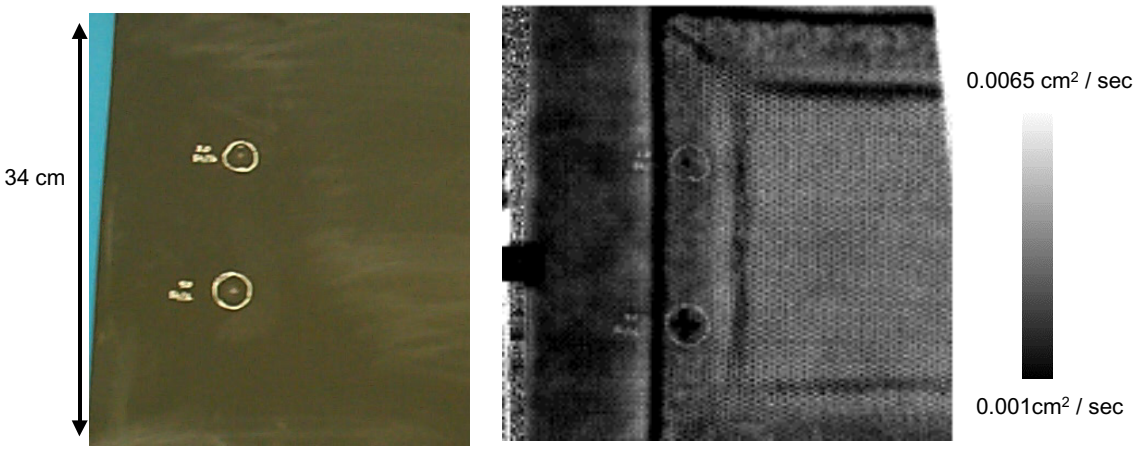

Figure 19: Visual and thermal diffusivity inspection image of left side impacts (area II).

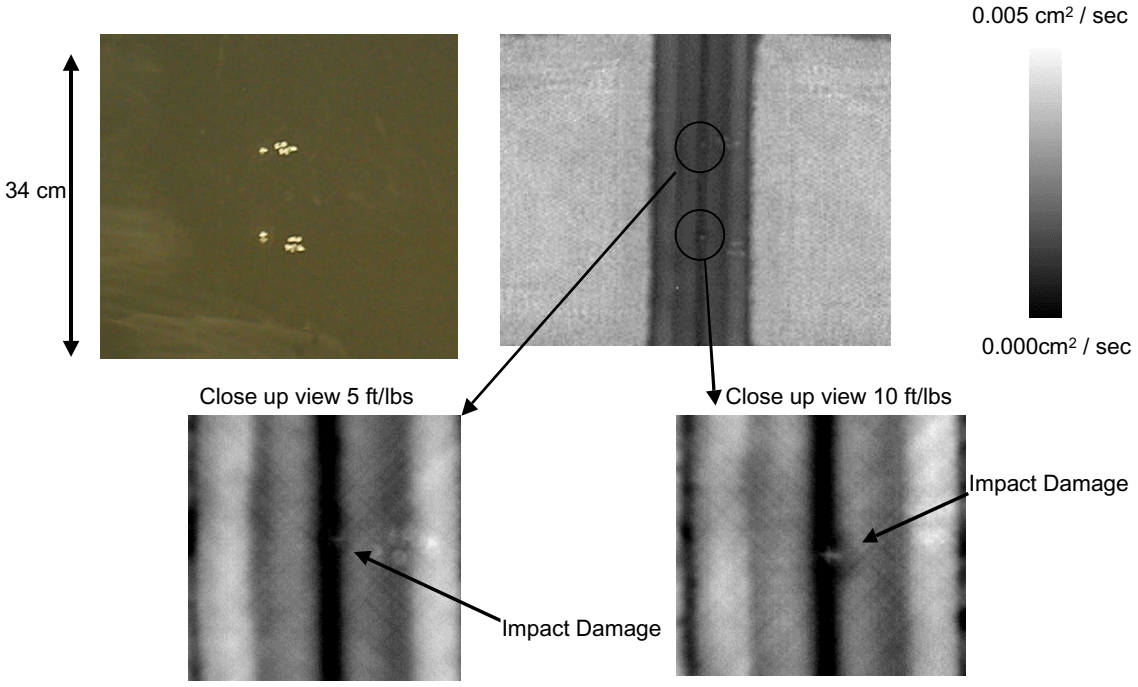

Figure 20: Visual and thermal diffusivity inspection image of middle impacts (area III).

Through Transmission Thermal Inspections

The through transmission thermal measurements of the double ramped sandwich panel with T-Blade were broken up into 2 inspection views (top and bottom) along the T-Blade center. The inspection of the 5 ft-lbs and 10 ft-lbs areas are shown in figures 21 and 22 respectively. The inspection parameters were 200 frames acquired at 60 frames per second for a total inspection time per view of 3.33 seconds. The smallest FEP insert was not detected due to the blade stiffener, however larger FEP inserts and both impact damage areas are detected as shown in figures 21 and 22. The impact damage is shown protruding to the right of the impact site and confirms the single side thermal measurements made previously.

The through transmission thermal measurements of the honeycomb core panel were performed using the quartz lamps. A quartz lamp was necessary to heat through the honeycomb. The inspection image is shown in figure 23. The inspection parameters were 64 frames averaged in real time (acquired at 30 frames per second) with 120 averaged frames for a total inspection time of 4.26 minutes. This long inspection time was required to allow the heat to transfer through the honeycomb core. The impact damage appears to be a higher diffusivity in figure 23 (lighter color) due to the crushed core/skin changing the thickness.

The X-Cor™ advanced sandwich panel was also inspected using the quartz lamps in through transmission mode. The inspection image is shown in figure 24. The inspection parameters were 16 frames averaged in real time (acquired at 30 frames per second) with 200 averaged frames for a total inspection time of 1.77 minutes. The impact damage areas and pull pin defects are shown as lower thermal diffusivity values (darker areas). By removing material the effective throught the thickness thermal diffusivity is lowered and therefore consistent with the lower values.

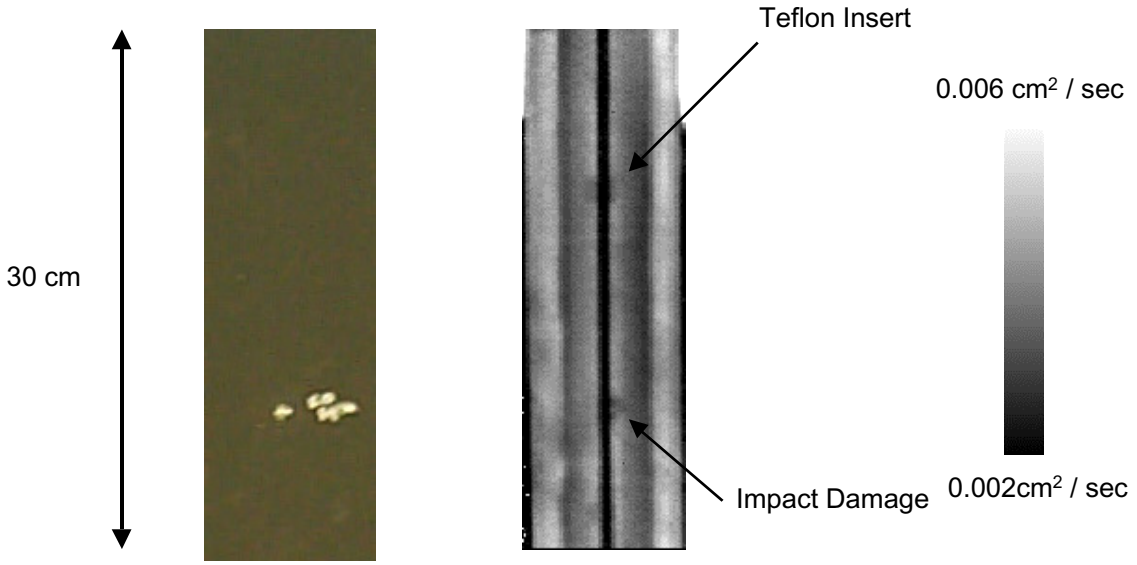

Figure 21: Thermal diffusivity inspection image of top T-Blade section (area III).

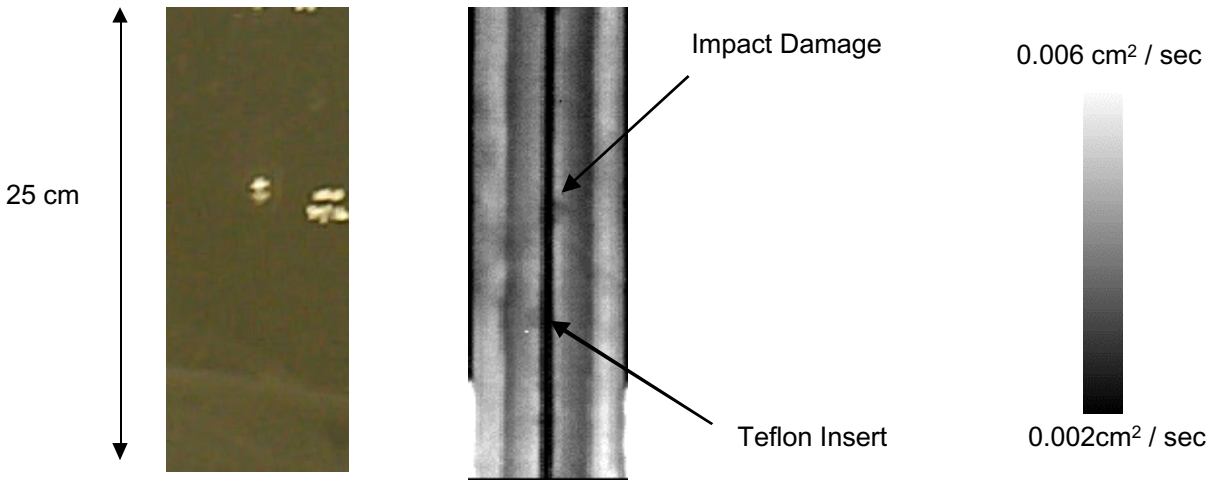

Figure 22: Thermal diffusivity inspection image of bottom T-Blade section (area III).

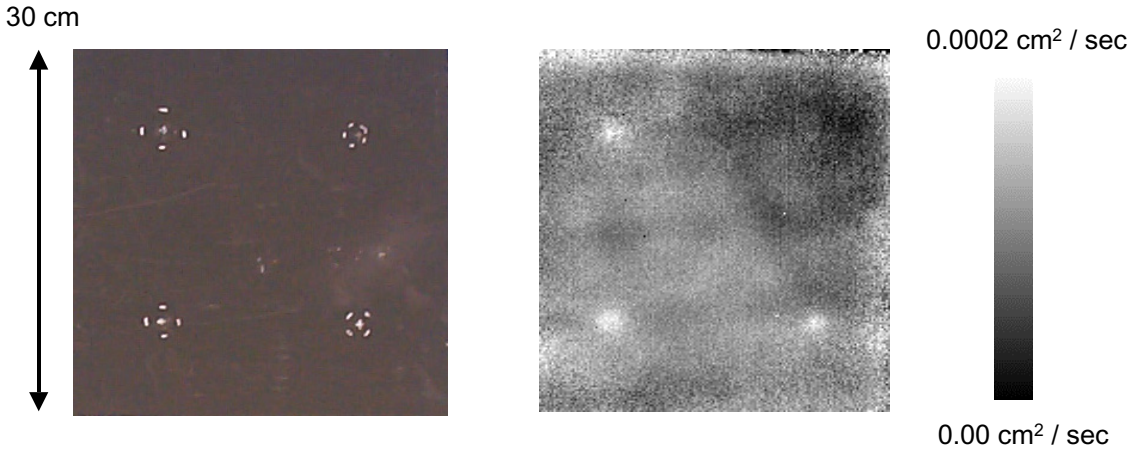

Figure 23: Thermal diffusivity quarz lamp inspection image of honeycomb core panel (area II).

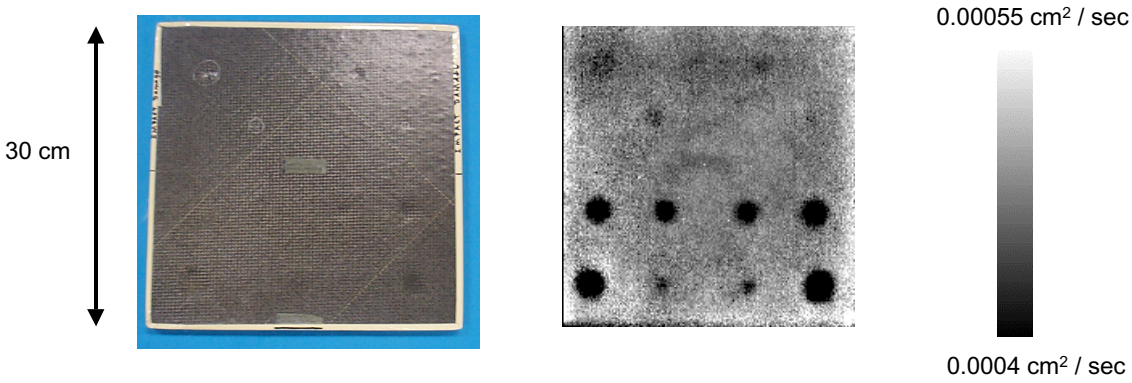

Figure 24: Thermal diffusivity quartz lamp inspection image of X-Cor™ advanced sandwich panel.

Discussion of Results

Single side and through transmission thermal inspections using flash and quartz heat lamps were performed on the samples provided by Sikorsky. For the composite honeycomb sample, all the foreign object inserts and impact damage defects were detected, although the smallest impact energy defects were barely detectable. The low reflectivity paint did not adversely effect the thermal inspection but enhanced it. This can be seen by comparing figures 9 and 10 where the honeycomb pattern is more clearly seen on the painted side. An image normalization data analysis technique was used on the data to detect foreign object inserts in the honeycomb core panel. The data analysis technique improved defect contrast and is faster than the model based thermal diffusivity imaging technique. The routine took 20 seconds to execute per data set. Through transmission thermal diffusivity image was generated on the honeycomb panel using a quartz lamp. The heat was able to propagate through the honeycomb. This is significant because the potential to detect damage on the opposite side from the heat source may be possible for honeycomb structures. The inspection image, shown in figure 23 was able to show the areas of impact damage by imaging changes in thickness due to the impact compression. All the impact damage and pull pin defects were detected on the X-cor™ advanced sandwich panel althought the smallest pull pin defects were more easily detected on the back side. Through transmission quartz lamp results easily detected all the pull pin defects, however the impact damage was barely detectable using this technique as shown in figure 24. The smallest T-blade side impact was not detected which could possibly indicate no damage. Close up single side thermal inspections were performed on the two impacted areas on the middle T-blade of the double ramped sandwich panel. The processed thermal diffusivity images were able to show the extent of damage around the T-blade. Through transmission thermal diffusivity images using the flash lamp was generated on the middle defects on the T-blade and compared well with previous measurements. The impact damage defects were clearly seen along with the largest foreign object inserts. The smallest foreign object inserts were not clearly seen due to the blade.

LASER ULTRASOUND

Laser based ultrasound is a non-contact inspection technology that uses a laser to generate ultrasound and a laser-interferometer system to measure ultrasonic surface vibrations [2,3]. The system used in this inspection incorporates fiber optics to transmit optical radiation to the specific area of inspection that can be easily shielded and thus protect personnel [7]. Other research laboratories are also employing fiber optics to extend and advance the utility of laser-based ultrasound [8, 9]. The use of fiber optics makes this system semi portable that can potentially be used in a large laboratory or depot type area with typical laser safety precautions. The objective of this inspection is to assess the use of laser-based ultrasound technology for inspection of structural composites for delaminations and or defects that maybe caused by impacts.

Laser ultrasonic generation and interferometric detection methods have been described in detail by other authors, [2,3,10,11,12]. Typically, laser pulses that rapidly heat a thin material surface layer generate ultrasound. This small heated volume expands creating stresses that act as a source of elastic waves in the material. The resulting surface displacement, u, in an isotropic material, using a simple one-dimensional model is given by [2],

$$u = \frac{(1+\nu)}{(1-\nu)} \frac{\alpha \delta E}{\rho C} \tag{1}$$

where ν is the Poisson's ratio, α is coefficient of linear expansion, δE is absorbed laser pulse energy assumed to have a uniform energy distribution, ρ is the material density, and C is the specific thermal capacity of the material. More complex models take into account thermal conductivity [13] and laser beam intensity distributions in orthotropic material [14]. Two additional mechanisms for generating ultrasound occur when material is melted or ablated by the laser, and when that material surface is constrained by paint or other thin layer. The amplitude of the elastic waves by both these methods can be 100 times greater then those generated by thermoelastic expansion. However, the ablation process damages the material and painting may not always be feasible. Therefore, the thermoelastic expansion mechanism is best suited for nondestructive evaluation.

Typical ultrasonic vibrations generated by normal piezoelectric or laser sources have a 1 to 50 nm amplitude and 100 kHz to 10 MHz frequency range. Backscatter of a probe laser beam is used to detect this ultrasonic vibration and convert it to an electronic signal. The vibrating surface causes the backscatter laser wavelength to be modulated by the vibrating surface. The Doppler effect describes how the wavelength of light reflected from the vibrating surface is shifted by an amount proportional to the surface velocity. This shifted wavelength, λ_s is given by

$$\lambda_s = \left(1 - 2\frac{\vee}{c}\right)^{-1} \lambda_0 \tag{2}$$

where $\vee$ is the velocity of the vibrating surface, c is the speed of light and λ_0 is the un-shifted laser wavelength. A Fabry-Perot Interferometer is typically the instrument of choice for

detecting and measuring the ultrasonic surface vibrations. The classic Fabry-Perot interferometer is composed of two partially reflecting mirrors separated to form a cavity. When light from the vibrating surface enters the cavity, multiple reflections are generated between the partial mirrors with some light transmitted and reflected out of the cavity. The relation governing the intensity of transmitted light, I_t, is [15]

$$I_t = \frac{(1-R)^2}{(1-R)^2 + 4R\sin^2(\phi)} I_i \qquad (3)$$

where I_i is the intensity of incident light, R is the reflectivity of the mirrors, and $\phi = (2\pi nL/\lambda_i)\cos\theta$ is the phase difference due to the mirror separation, in which n is the index of refraction of the cavity, L the is cavity length or mirror separation, λ_i is the incident optical wavelength, and θ is the angle of incidence of light upon the mirror. Optical detectors transform the intensity changes of the transmitted light into a voltage signal. This voltage signal resembles a typical ultrasonic waveform from conventional ultrasonic transducers that can be digitized and evaluated.

System Description

Major components of the laser-based ultrasonic system include generation and detection lasers, Fabry-Perot interferometer, and optical components. Other components consist of a PC computer, oscilloscope for data acquisition, and x-y scanning bridge and controller. A picture of the system in figure 25 shows lenses on an x-y scanning bridge and in the background an optical table containing the lasers and Fabry-Perot Interferometer. The total system cost is approximately $200K. The generation and detection lasers in this system are both Nd:YAG lasers. The generation laser is a Q-switched pulsed laser with a wavelength of 1064nm, and has variable pulse energy up to 200 mJ with pulse duration of 20nsec. This pulse width produces ultrasound with a center frequency of about 5MHz. The detection laser is a continuous wave laser with a wavelength of 532 nm, beam diameter of 0.32 mm, maximum output power of 400mW, and a line stability of less then 10kHz. The light from the lasers and light traveling from the material under inspection to the interferometer are completely contained within, a 60-foot length, fiber optic cables that runs from the lasers on the optical table to the lenses on the scanning bridge. Light from the generation laser travels through the fiber optic cable to a lens on the x-y scanning bridge. This lens focuses the laser light onto the surface of the material being inspected. The generation laser pulse creates ultrasonic waves that travel in the material being inspected. Light from the detection laser travels through the fiber optic cable to a second lens on the x-y scanning bridge. This second lens focuses the laser light onto the surface of the sample being inspected. This light is reflected and scattered from the surface. Part of the reflected and scattered light is collected by a third lens, on the x-y scanning bridge, that transmits the light to the Fabry-Perot Interferometer via fiber optic cable. The distance between the lenses on the x-y scanning bridge and the material under inspection is approximately 25 centimeters. A PC-based virtual instrument controls the scanning stage and stores the ultrasonic signals for later processing

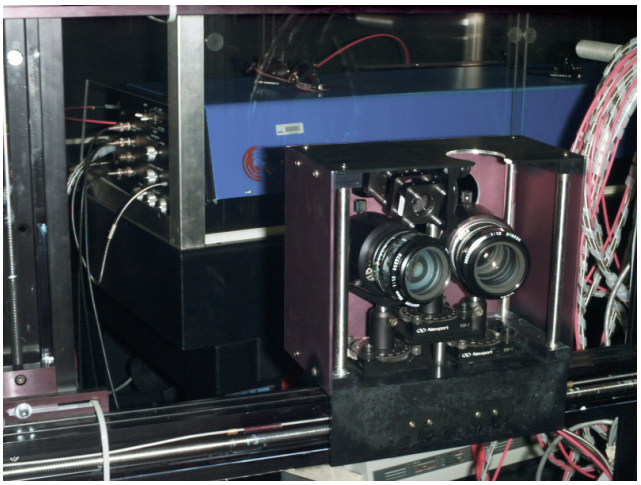

Figure 25: Laser Based Ultrasound System with lens on a x-y scanning bridge and optical table in background with Fabry-Perot Interferometer and lasers.

Discussion of Results

The specimens tested with laser-based ultrasound were the sandwich honeycomb core sample and the double ramped T-blade sample. A third sample was a 6-ply woven graphite sample used to evaluate the laser damage threshold. Damage evaluation was also carried out on the sandwich honeycomb core sample. Damage thresholds tests were conducted on the bare surface of a woven-graphite sample and the black surface of the sandwich honeycomb core panel to evaluate possible damage to the material from the lasers used in the inspection process. As noted earlier, the lasers used are both Nd:YAG lasers with the generation laser being a pulsed laser with a wavelength of 1064nm and the detection laser a continuous wave laser with a wavelength of 532nm. Generation laser tests on the 6-ply woven graphite sample showed the threshold of damage to be between 10 and 15 mJ/pulse with a 5mm diameter spot size. The damage appears as a dull spot on a shiny surface. Figure 26 shows pictures of this sample with the damage resulting from a single laser pulse (bottom picture) and multiple laser pulses (top picture). On closer inspection the fibers in the damage area seem to be more readily seen than in other areas of the sample. It is possible there is some fiber/matrix de-bonding. The matrix material may be transparent to the laser generation wavelength of 1064nm and thus the fibers are directly heated causing the de-bonding and/or a brightening in the fibers. Similar tests on the sandwich honeycomb core panel showed the threshold of damage at approximately the same level as on the bare graphite sample. Laser pulse energies of 1, 2, 5, and 10mJ/pulse were used to test for damage. The appearance of damage became questionable at the 10mJ/pulse level when a very slight discoloration in the surface could be seen. Detection laser tests on both samples showed no visible damage for a power of 150 Watts with a 2mm-diameter laser beam.

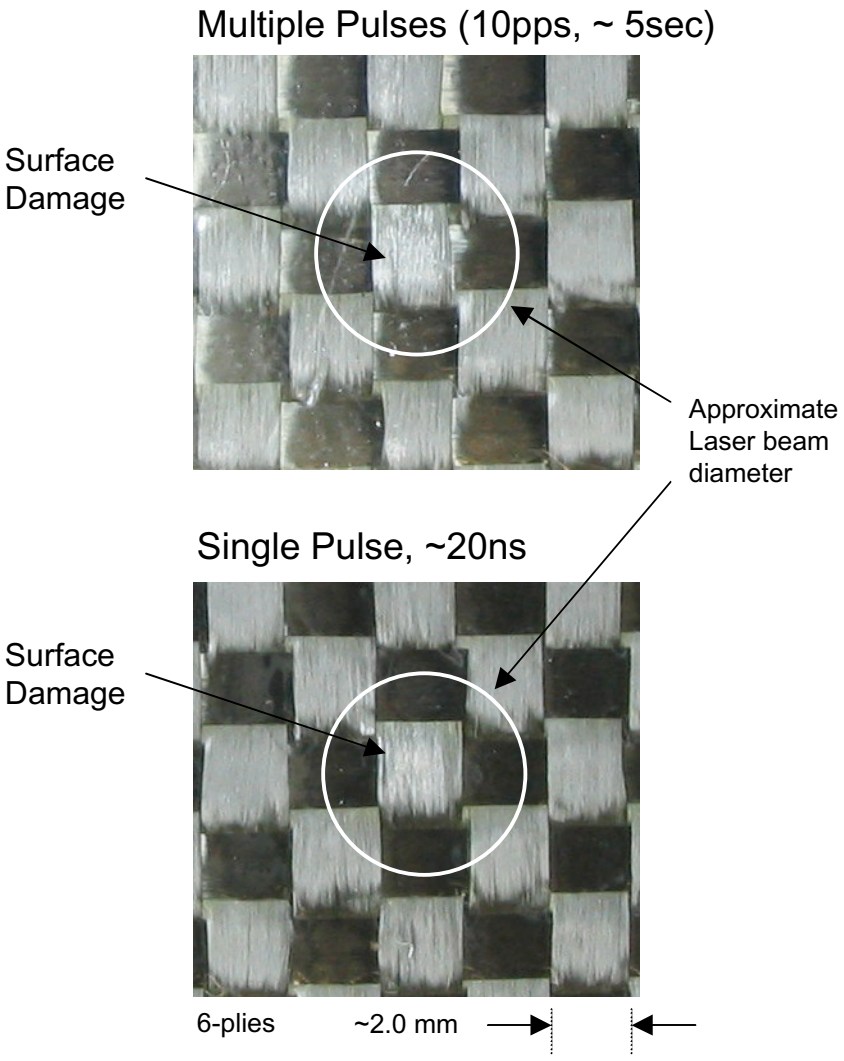

Figure 26: Damage threshold tests on the bare surface of a woven-graphite sample. A Nd:YAG laser with a wavelength of 1064nm, 5mm beam diameter, pulse duration of approximately 20ns, and laser power of approximately 20mJ/pulse was used.

An area of the sandwich honeycomb core panel was prepared for laser based ultrasonic inspection by applying a thin layer of vacuum grease in about a 7.6 centimeters square area around an impact site. The vacuum grease enhances the generation of ultrasound for the 1064nm wavelength, by acting as a constraining layer. Enhancements of around 25dB were demonstrated

with the application of light oil [2]. The vacuum grease also acted as a reflective coating for the 532nm wavelength and thus provided more light for the interferometer measurement. A picture of the sample, in front of the laser-based ultrasound lens system is shown in figure 27. The darker area is the inspection area with the thin layer of vacuum grease. In the foreground the lens on the x-y scanning bridge can be seen. This impact had a dent with a diameter of ~20mm and a depth of ~2mm. The general location and expanded view of the inspection area is shown schematically in figure 28. The approximate location of the inspection points is shown in a series of horizontal and vertical points across the impact area. Spacing is 0.254 centimeters points across the impact area. The ultrasonic signature from these points across the inspection area did not show major variations as would be expected from delaminations occurring in the outer skin. This could in part be due to damage being near the front surface and the ultrasonic reflections being obscured by the initial impulse from the laser. A sample of the ultrasonic signature is shown in figure 29.

The Double Ramped T-blade panel was inspected across the T-blade area with laser-based ultrasound. The first area inspected was around the 10 ft-lb impact site. The area scanned was 8.9 centimeters wide by 6.4 centimeters in height with 0.254 centimeters increments between inspection points. The ultrasonic waveforms were processed to generate a time-of-flight C-scan image. Figure 30 shows the position of the inspection area around the 10 ft-lb impact site and figure 31 shows the T-blade profile and the time-of-flight C-scan. Thickness changes in the T-blade correspond to color changes in the C-scan. A loss of signal echo was observed for the web/fillet area of the T-blade and is seen as a vertical strip in the center of the scan area. In the center of the scan is a circular area, approximately 1.9 centimeters wide by 1.0 centimeters high, this is the damage area around the the 10 ft-lb impact. Additional sections were scanned with

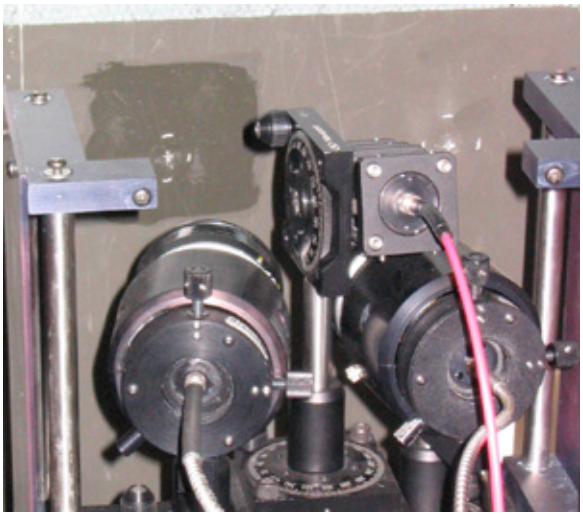

Figure 27: A picture of the sandwich honeycomb core composite panel located in front of the laser-based ultrasound lens system is shown.

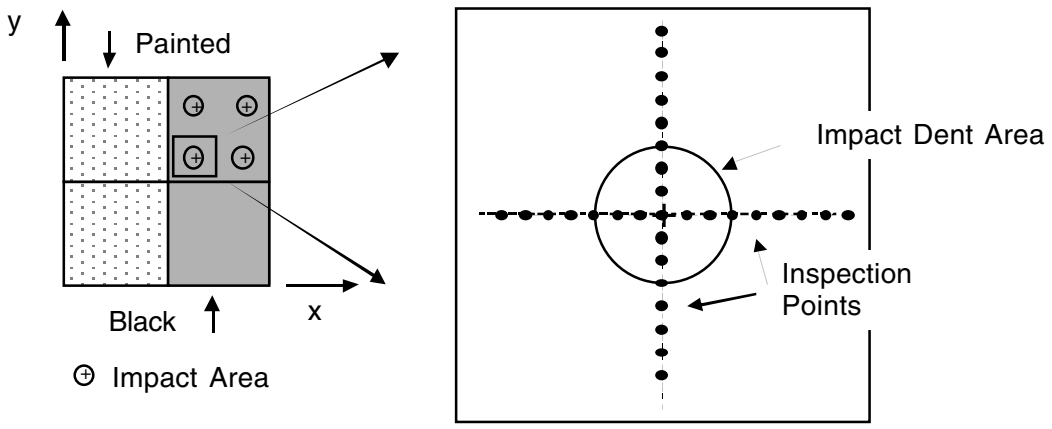

Figure 28: A schematic of the sandwich honeycomb core composite panel shows the general location of the impacts and an expanded view of the inspection area.

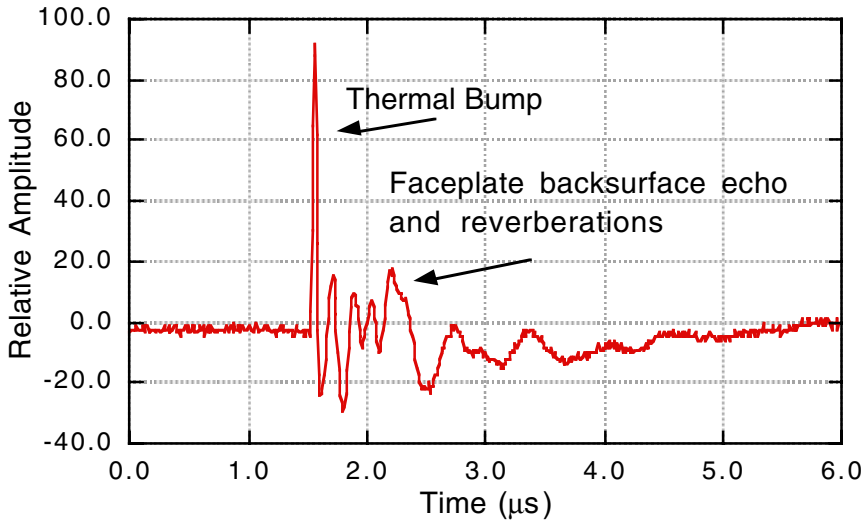

Figure 29: A sample ultrasonic signature composed of an initial pulse caused by the generation laser impulse and followed by an ultrasonic echo from the faceplate back surface and possibly some echo reverberations.

the same dimensions and incremental spacing. The processed images were then pasted together to form a composite image. This composite image included the 10 ft-lb impact and the area below it, almost to the edge of the sample. The composite C-scan is shown in Figure 32 and covers an area 8.9 centimeters wide by 22.8 centimeters high. This image shows the loss of echo in the T-blade web area, the 10 ft-lb impact, and two embedded defects. Scans around the 5 ft-lb

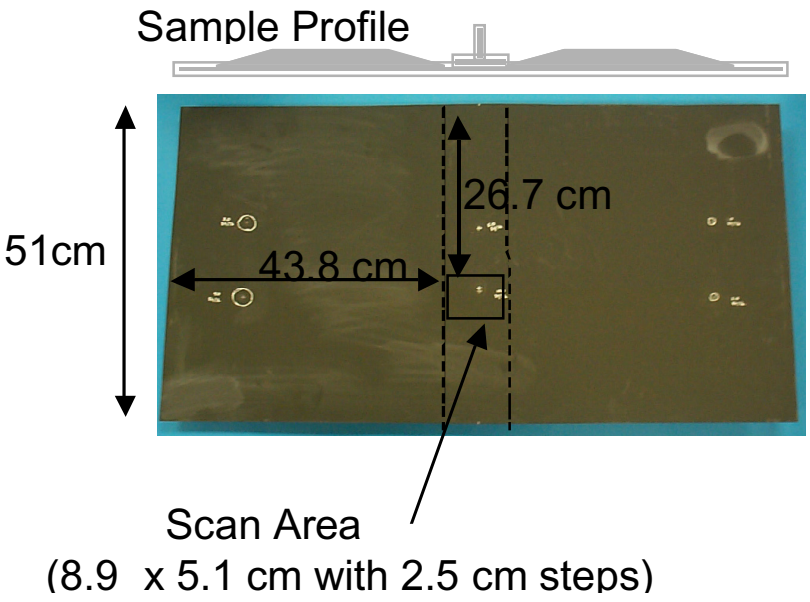

Figure 30: Position of the scan area around the 10 ft-lb impact site is shown.

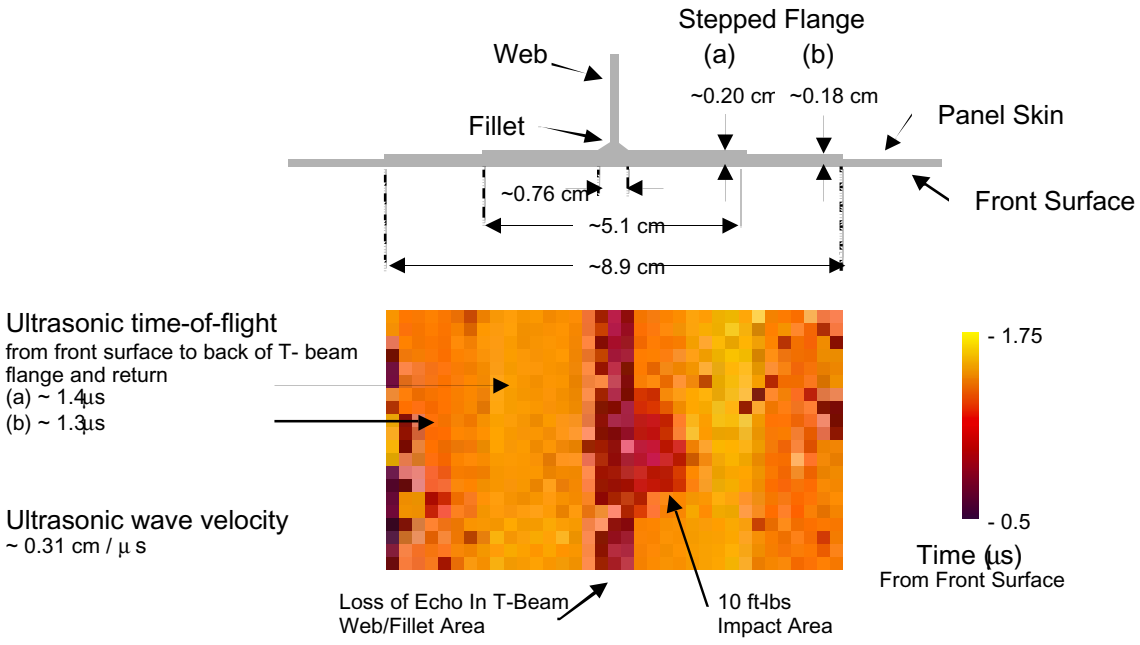

Figure 31: T-blade profile and time-of-flight C-scan around the 10 ft-lb impact site.

impact were conducted and again a composite image was obtained. The composite C-scan is shown in Figure 33 and covers an area 8.9 centimeters wide by 24.1 centimeters high. This image shows the loss of echo in the T-blade web area, two embedded defects, and the 5 ft-lb impact. These images showed that the general structure in the T-blade could be seen in the generated C-scan images and that it was possible to observe 0.025 centimeters thickness changes in this structure. Inserts near the T-blade flange back surface were readily seen, but inserts near the flange front surface were obscured in part from the laser ultrasound generation. The impact damage area for the 10 ft-lb site was readily seen, but the damage area for the 5 ft-lb impact site was not well defined. In this later area damage may be near the front surface and partially hidden by the laser ultrasound generation signal. In general the laser-based ultrasound appears to be a viable method for inspecting the T-blade for thickness variations and more extensive impact damage.

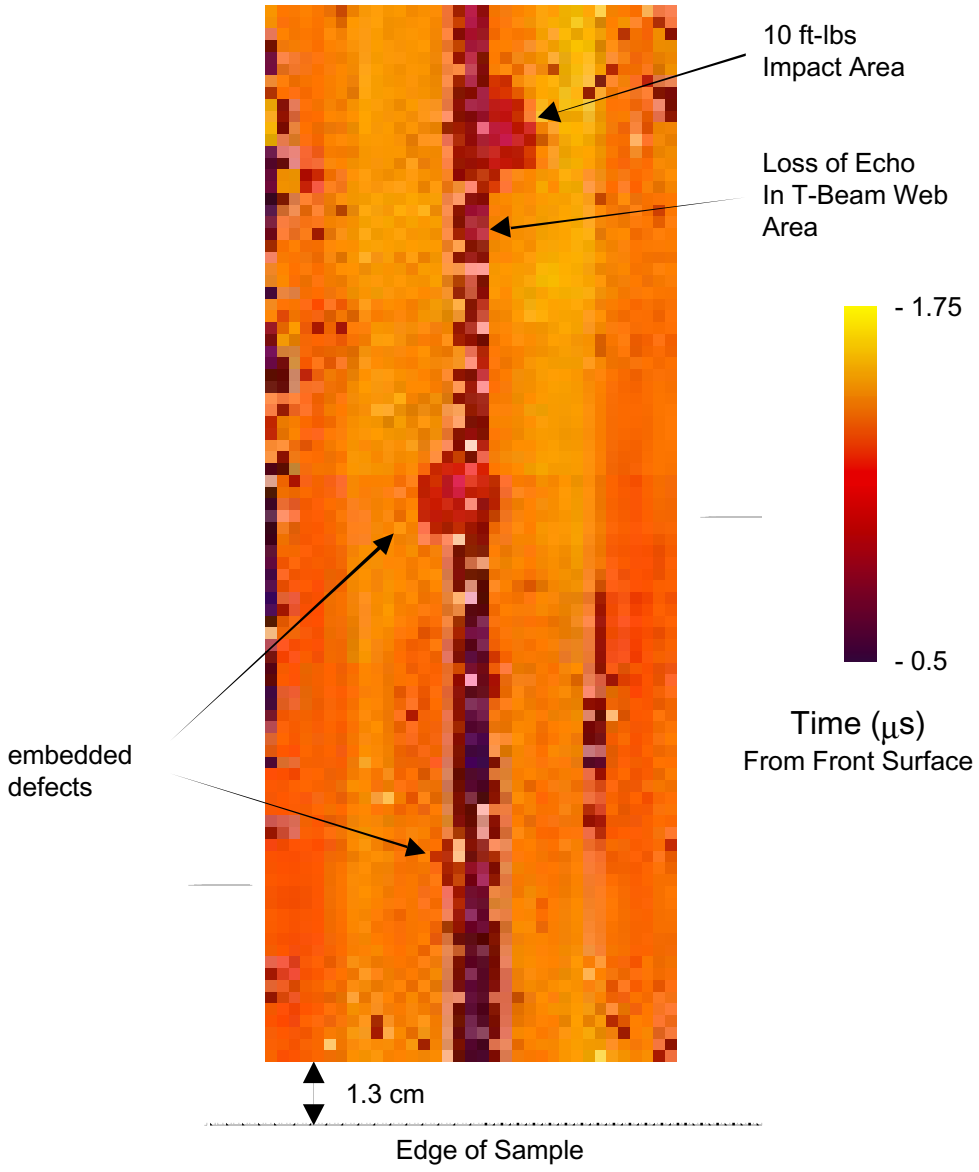

Figure 32: Time-of-flight C-scan image showing the loss of echo in the T-blade web area, the 10 ft-lb impact, and two embedded defects. The scan area is 8.9 x 22.9 centimeters.

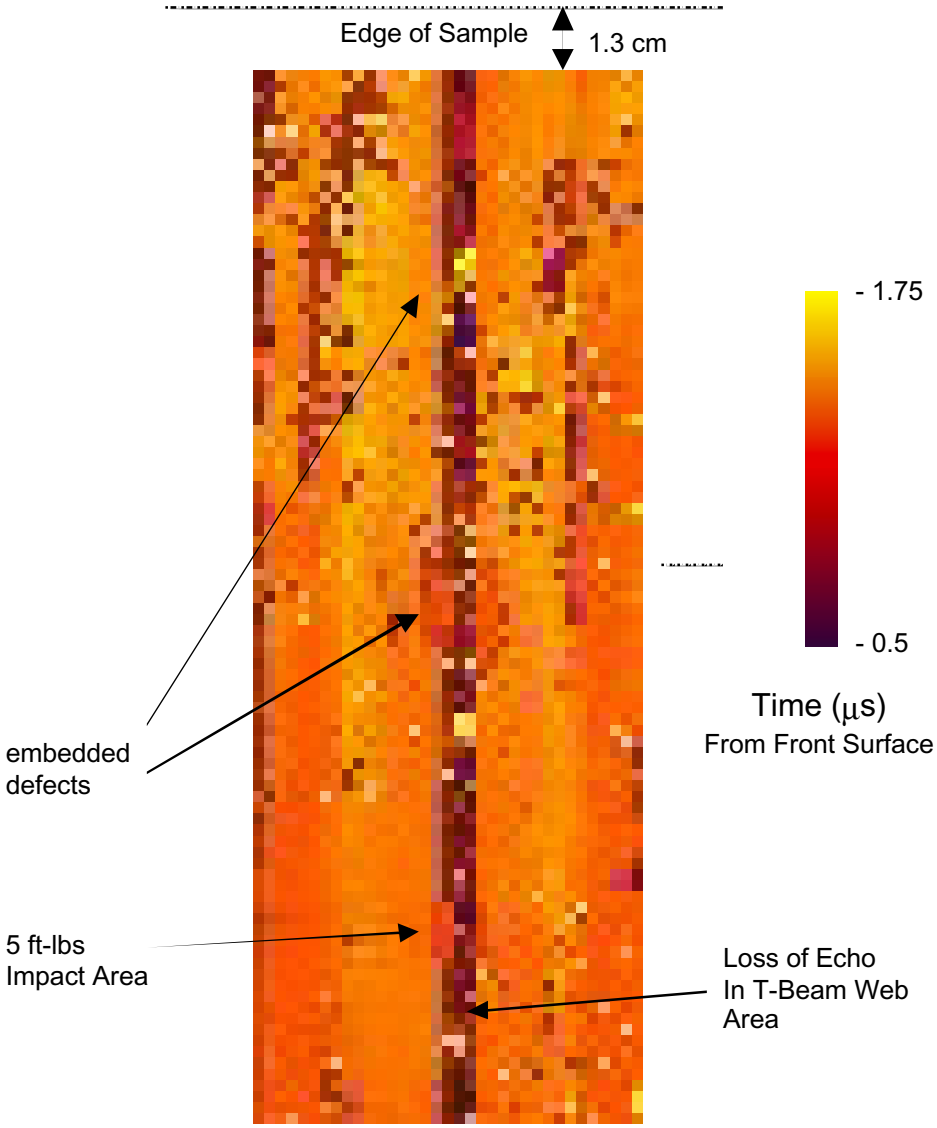

Figure 33: Time-of-flight C-scan image showing the loss of echo in the T-blade web area, two embedded defects, and the 5 ft-lb impact. The scan area is 8.9 x 24.1 centimeters.

ULTRASONIC LAMB WAVE

Lamb waves are guided waves formed by the interference of multiple reflections and mode conversions of longitudinal and shear waves at the free surfaces of a plate [16-18]. These waves are typically generated and detected using conventional piezoelectric transducers, oriented either flat or at an angle with respect to the surface. Lamb waves are used to detect defects and measure elastic properties of thin isotropic materials and laminated composite plates. For material-property measurements dispersion curves are reconstructed from experimental measurements of phase velocity as a function of frequency. Ultrasonic Lamb or surface waves have an advantage over conventional through-the-thickness ultrasound because the energy can be transmitted over greater distances.

Background

Lamb waves or guided waves refer to a type of ultrasonic wave propagation in which the wave is guided between two parallel surfaces of the test object and have a frequency dependent velocity. Two groups of waves propagate, these are the symmetric group and the anti-symmetric group and each group propagates with multiple modes. By solving a boundary value problem for a free plate or by considering the reflection of waves at plate boundaries the Rayleigh-Lamb dispersion equations can be obtained. These equations for a uniform isotropic plate are [16-18]

$$\frac{\tan\left(\beta\frac{d}{2}\right)}{\tan\left(\alpha\frac{d}{2}\right)} = -\left[\frac{4\alpha\beta k^2}{\left(k^2-\beta^2\right)^2}\right]^m \tag{4}$$

where

$$\alpha^2 = \frac{\omega^2}{c_L} - k^2 \tag{5}$$

$$\beta^2 = \frac{\omega^2}{c_T} - k^2 \tag{6}$$

where d is plate thickness, $\omega = 2\ \pi\ \mathrm{f}$ is the circular frequency, $\mathrm{k} = \omega / c$ is the wave number, c is the Lamb wave phase velocity, c_L is the longitudinal wave velocity, c_T is the shear wave velocity, and the exponent, m, in equation (4) has the value +1 for symmetric modes and –1 for anti-symmetric modes of wave propagation. Longitudinal and shear wave velocities are related to the material's elastic properties by [16-18]

$$c_L = \sqrt{\frac{E}{\rho}\frac{(1-\upsilon)}{(1+\upsilon)(1-2\upsilon)}} \tag{7}$$

$$c_T = \sqrt{\frac{E}{\rho}\frac{1}{2(1+\upsilon)}} \tag{8}$$

where E is Young's modulus, υ is Poisson's ratio, and ρ is density.

The phase velocity in the dispersion equations is found numerically by solving for the real roots of the equation as a function of material properties, frequency, and material thickness. For an aluminum plate with a 1.016 mm thickness the first and second symmetric (s_0 and s_1) and first and second anti-symmetric (a_0 and a_1) modes are shown in figure 34. It can be seen that at very low frequencies the wave velocity of the first symmetric mode is nearly non-dispersive while the wave velocity of the first anti-symmetric mode is highly dispersive. At higher frequencies the phase velocity of both zero order modes approach the Rayleigh wave velocity. For aluminum (υ = 0.33) this velocity is 2.9 km/s [16].

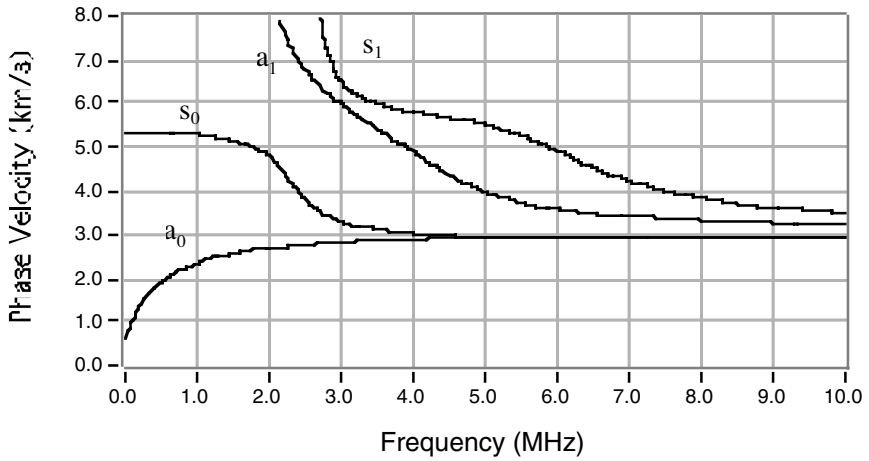

Figure 34: First and second symmetric (s_0, s_1) and asymmetric (a_0, a_1) dispersion curves in a 1.016mm thick aluminum plate.

System Description

The ultrasonic Lamb wave system used is shown in figure 35. This figure shows a schematic with two transducers on a material surface, one generating ultrasonic Lamb waves and one receiving and a picture of the system. The system used is commercially available from Digital Wave Corporation. The system consists of an x-y scanning bridge, scanner control unit,

function generator and A/D capture boards. The total system cost is approximately $50K. The transducers used for both pitch and catch are wide bandwidth (50 KHz – 1.5 MHz) and displacement sensitive.

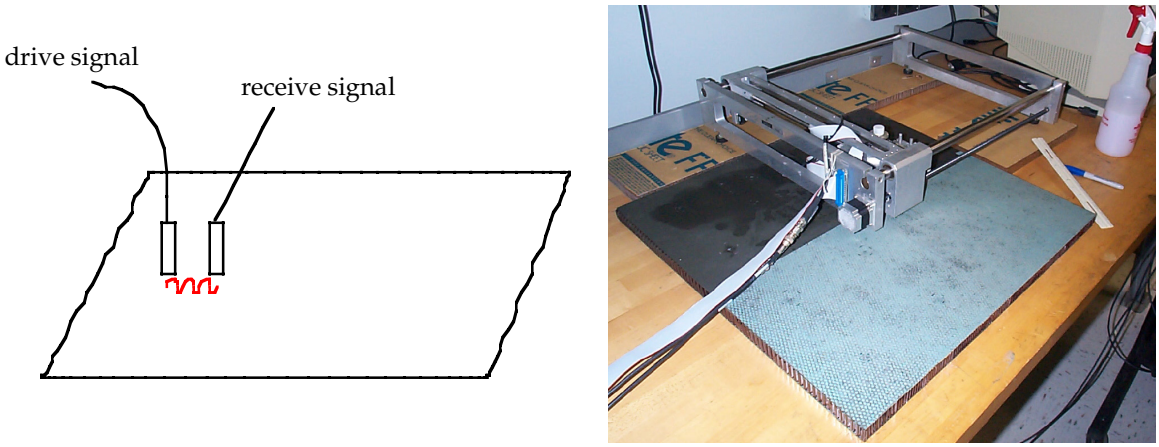

Figure 35: Schematic (left) and picture (right) of setup used for ultrasonic Lamb wave measurement. The schematic show two transducers on a material surface with the drive transducer generating ultrasonic Lamb waves and the receiving transducer located a short distance away.

Discussion of Results

The specimens tested with the ultrasonic Lamb wave system were described earlier in this report. These were the sandwich honeycomb core panel, X-Cor™ advanced sandwich panel, and the double ramped T-blade panel. The panels were scanned in sections approximately 30 by 30 centimeters with 2.5 centimeters incremental steps. The drive signal generated was a Gaussian modulated sine wave with a 50kHz frequency. The received transducer was located 2.54 centimeters from the drive transducer. The received signal was digitized to an eight-bit resolution at a 25MHz-sampling rate with 4096 point per waveform. The signals were stored on computer disk for post processing. On each scan amplitude measurements were performed on the signals. In this processing a peak in the received signal was selected and its location gated with a sampling window. The amplitude in this sampling window was recorded as a function of location and an amplitude C-scan was generated. The amplitude in part corresponds to the material characteristics between the transmitting and receiving transducers. Material characteristics include thickness variations, elastic property changes, and changes due to defects and inclusions. The C-scan images of the scanned sections were pasted together to form a composite C-scan image. Figures 36, 37, and 38 show pictures of the panel and C-scan image of the X-Cor™ advanced sandwich panel, the sandwich honeycomb core panel, and the double ramped T-blade panel, respectively. In these C-scan images the darker areas correspond to some form of material change with some of the areas corresponding to the known damage and inclusion areas. It is possible that more conclusive results could be obtained by varying the drive signal frequency and amplitude or optimizing transducer size.

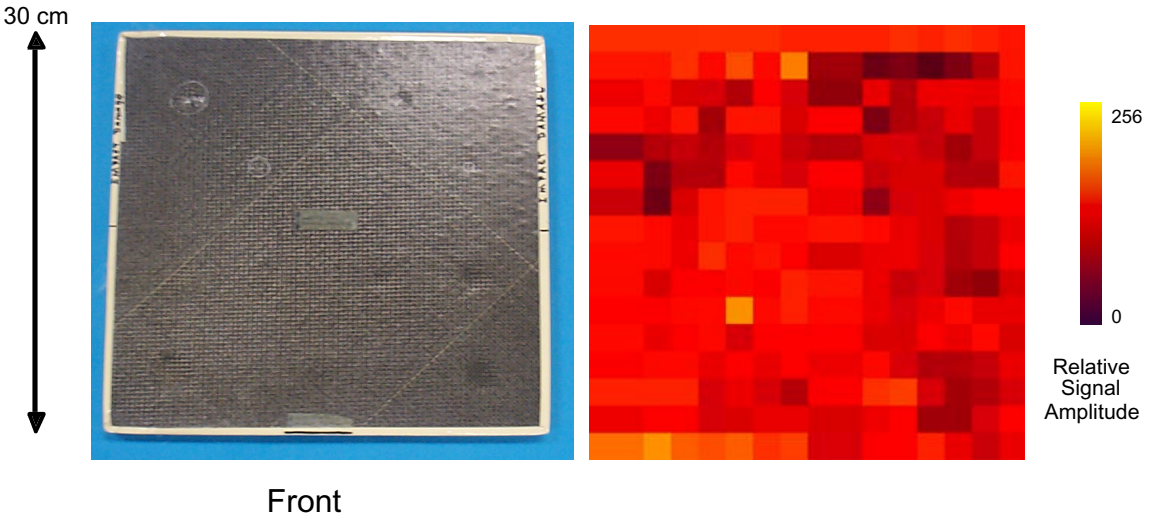

Figure 36: Picture of X-Cor™ advanced sandwich panel (top) and amplitude C-scan image.

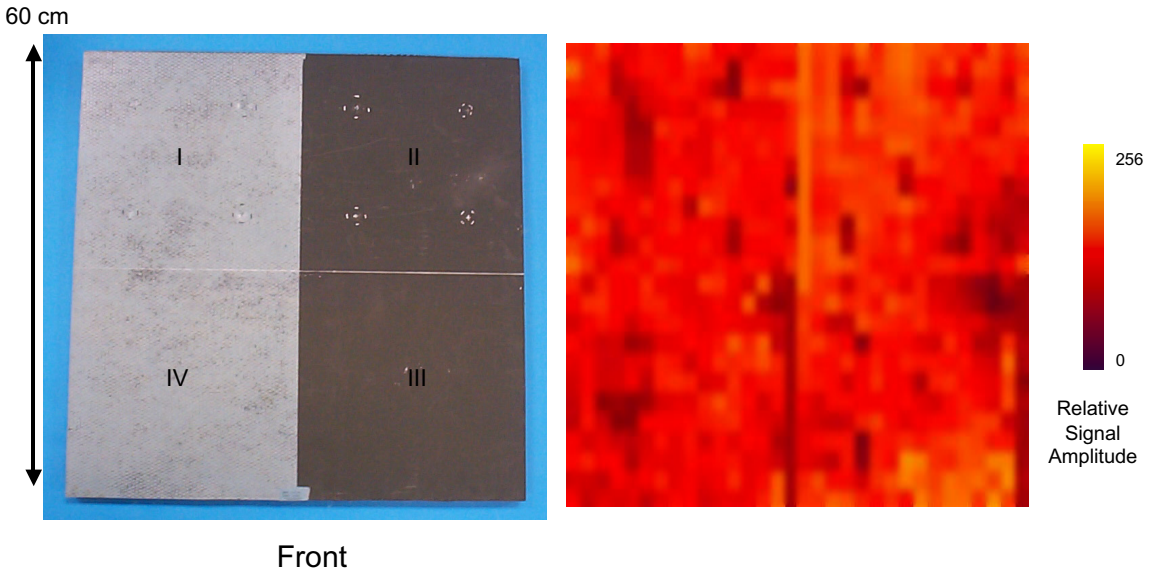

Figure 37: Picture of honeycomb core panel (top) and amplitude C-scan image.

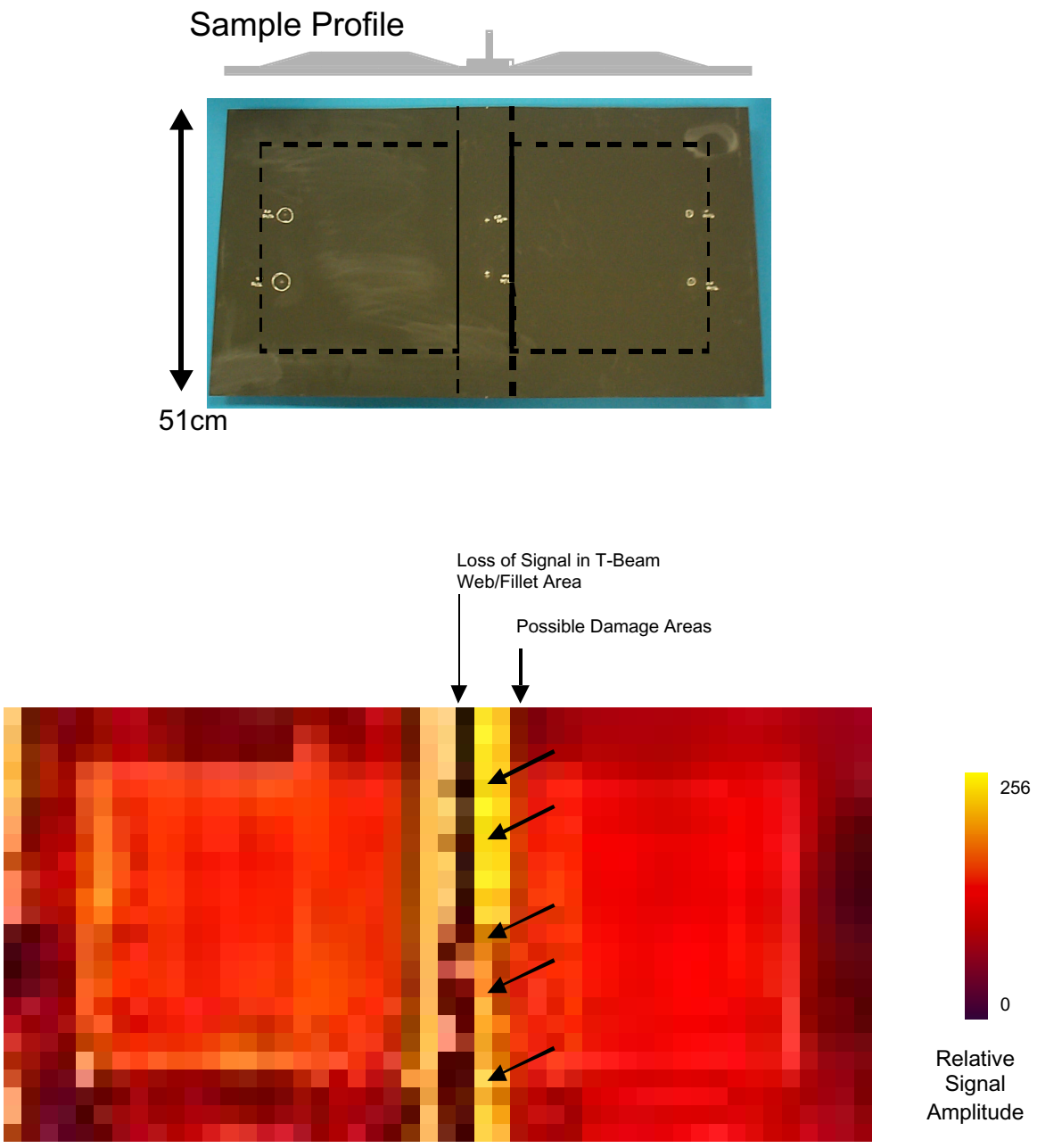

Figure 38: Picture of Double Ramped T-blade panel (top) and amplitude C-scan image.

CONCLUSIONS

Based on the overall results obtained in this study, thermography proved best because of its ability to detect the defects of interest as compared to the other technologies. In addition to thermography's field portability capability, the inspection technology is safe, one sided, noncontact and provides rapid full field imaging. Laser ultrasound was not able to inspect the samples with thin skins. Laser ultrasound has possibilities in limited applications, however field portability issues may restrict the technology to depot applications. Recent advances in miniature laser diode technology may result in future field portable systems. The ultrasonic Lamb wave technique gave the weakest results. Ultrasonic Lamb wave measurements of the double ramped T-stiffener area showed possible defect locations, however the lack of defect contrast on the other samples was disappointing. It is noted that the frequency selection and scanning resolution may have attributed to this. Lamb wave measurements were particularly difficult on samples with thin skins because of the low frequencies used. Since existing equipment was used, transducers more suited for thicker structures were only available. By optimizing the frequency and transducer size improved defect contrast could possibly be obtained.

REFERENCES

1. Winfree, W. P., Heath, D. M., "Thermal Diffusivity Imaging of Aerospace Materials and Structures", Thermosense XX, edited by J. R. Snell and R. N. Wurzbach, SPIE Proceedings Vol. 3361, Bellingham, WA, 1998 pp. 282-290.
2. Scruby C.B., and Drain L.E., Laser Ultrasonics: Techniques and Applications, Adam Hilger, New York, 1990.
3. Hutchins D.A., Ultrasonic Generation by Pulsed Lasers, Physical Acoustics. Vol. 18, 1988.
4. Seale M. D., Smith B. T., Prosser W. H., and Zalameda J. N., "Lamb Wave Assessment of Fiber Volume Fraction in Composites", J. Acoust. Soc. Am. 104 (3), Pt. 1, September 1998.
5. Zalameda J. N. and Winfree W. P., "Quantitative Thermal Nondestructive Evaluation Using an Uncooled Microbolometer Infrared Camera", Proceedings of SPIE, Volume 4710, April 1-5, 2002 pages 610-617.
6. Zalameda J. N., Farley G. L., and B. T. Smith, "A Field Deployable Nondestructive Impact Damage Assessment Methodology for Composite Structures," American Society for Testing and Materials Journal of Composites Technology and Research, Vol 16, Number 2, April 1994, pp. 161 - 169.
7. Anastasi, R.F., A.D. Friedman, M.K. Hinders, and E.I. Madaras, "NDE of Damage in Thick Stitched Composites Using Laser-Based Ultrasound with Optical Fibers," Materials Evaluation, Vol. 56, No. 12, December 1998
8. McKie, A.D.W. and R.C. Addision Jr., *Progress Toward a Fiber-Based Laser-Ultrassonic System for Rapid NDE of Large Area Composites*, Review of Progress in Quantitave Nondestructive Evaluation, Vol. 16, Edited by D.O. Thompson and D.E. Chimenti, Plenum Press, New York, 1997
9. Wang, Luui-Shen, J.S. Steckenrider, and J.D. Achenbach, *A Fiber-Based Laser Ultrasonic System for Remote Inspection of Limited Components*, Review of Progress in Quantitave

Nondestructive Evaluation, Vol. 16, Edited by D.O. Thompson and D.E. Chimenti, Plenum Press, New York, 1997
10. Monchalin, J.-P. and R. Heon, "Laser Ultrasonic Generation and Optical Detection with a Confocal Fabry-Perot Interferometer," *Materials Evaluation*, Vol. 44, September 1986.
11. Wagner, J.W., *Optical Detection of Ultrasound*, Physical Acoustics, Vol. XIX, Academic Press, 1990.
12. Monchalin, J.-P., R. Heon, P. Bouchard, and C. Padioleau, "Broadband Optical Detection of Ultrasound by Optical Sideband Stripping with a Confocal Fabry-Perot," *Applied Physics Letters*, 55(16), October 1989.
13. Telschow, K.L. and R.J. Conant, "Optical and Thermal Parameters Effect on Laser-Generated Ultrasound," *J. Acoust. Soc. Am*., 88(3), September 1990.
14. Dubois, M., F. Enguehard, M. Choque, J.-P. Monchalin, and L. Bertrand, "Numerical Modeling of Laser Generation of Ultrasound in Orthotropic Materials," in *Review of Progress in Quantitative Nondestructive Evaluation*, Vol. 13, Edited by D.O. Thompson and D.E. Chimenti, Plenum Press, New York, 1994.
15. Born, M. and E.Wolf, *Principles of Optics*, Pergamon Press, New York, 1964.
16. Auld, B.A. "Acoustic Fields and Waves in Solids, Volume II," Robert E. Krieger Publishing Company, Florida, 1990.
17. Achenbach, J.D., "Wave Propagation in Elastic Solids," Elsevier Science Publishers, New York, 1999.
18. Viktrorov, I.A., "Rayleigh and Lamb Waves," Plenum Press, New York, 1967. Bedford, A. and Drumheller, D.S., "Introduction to Elastic Wave Propagation," John Wiley and Sons, New York, 1994.

REPORT DOCUMENTATION PAGE

Form Approved
OMB No. 0704-0188

1. REPORT DATE *(DD-MM-YYYY)*	2. REPORT TYPE	3. DATES COVERED *(From - To)*
01- 08 - 2004	Technical Memorandum	

4. TITLE AND SUBTITLE

Nondestructive Evaluation (NDE) Results on Sikorsky Aircraft Survivable Affordable Reparable Airframe Program (SARAP) Samples

5a. CONTRACT NUMBER

5b. GRANT NUMBER

5c. PROGRAM ELEMENT NUMBER

6. AUTHOR(S)

Zalameda, Joseph N.; Anastasi, Robert F.; and Madaras, Eric I.

5d. PROJECT NUMBER

5e. TASK NUMBER

5f. WORK UNIT NUMBER

23-762-55-TF

7. PERFORMING ORGANIZATION NAME(S) AND ADDRESS(ES)

NASA Langley Research Center
Hampton, VA 23681-2199

U.S. Army Research Laboratory
Vehicle Technology Directorate
NASA Langley Research Center
Hampton, VA 23681-2199

8. PERFORMING ORGANIZATION REPORT NUMBER

L-19014

9. SPONSORING/MONITORING AGENCY NAME(S) AND ADDRESS(ES)

National Aeronautics and Space Administration
Washington, DC 20546-0001

10. SPONSOR/MONITOR'S ACRONYM(S)

NASA

11. SPONSOR/MONITOR'S REPORT NUMBER(S)

NASA/TM-2004-213235 ARL-TR-3130

12. DISTRIBUTION/AVAILABILITY STATEMENT

Unclassified - Unlimited
Subject Category 35
Availability: NASA CASI (301) 621-0390 Distribution: Nonstandard

13. SUPPLEMENTARY NOTES

This research was supported and partially funded by Sikorsky Aircraft and the Aviation Applied Technology Directorate under Technology Investment Agreement No. DAAH10-02-2-0001.
An electronic version can be found at http://techreports.larc.nasa.gov/ltrs/ or http://ntrs.nasa.gov

14. ABSTRACT

The Survivable, Affordable, Reparable Airframe Program (SARAP) will develop/produce new structural design concepts with lower structural weight, reduced manufacturing complexity and development time, increased readiness, and improved threat protection. These new structural concepts will require advanced field capable inspection technologies to help meet the SARAP structural objectives. In the area of repair, damage assessment using nondestructive inspection (NDI) is critical to identify repair location and size. The purpose of this work is to conduct an assessment of new and emerging NDI methods that can potentially satisfy the SARAP program goals.

15. SUBJECT TERMS

Lamb wave ultrasound; Laser ultrasound; Thermography; Composite defect detection; Large area inspection

16. SECURITY CLASSIFICATION OF:			17. LIMITATION OF ABSTRACT	18. NUMBER OF PAGES	19a. NAME OF RESPONSIBLE PERSON
a. REPORT	b. ABSTRACT	c. THIS PAGE			STI Help Desk (email: help@sti.nasa.gov)
					19b. TELEPHONE NUMBER *(Include area code)*
U	U	U	UU	40	(301) 621-0390